Dear Editor,

We are very grateful to the three referees for their appropriate and constructive suggestions and for their proposed corrections to improve the paper. We have addressed all issues raised and have modified the paper accordingly. If you and the referee agree on that, we are also ready to submit a revised version of the paper where all these changes have been introduced. We believe that, thanks to their precious inputs, the manuscript has now sensitively improved. Below is a summary of the changes we made and our specific responses to the referees' comments and recommendations.

Summary of the changes

(in black is the original comments of the referee and in red our responses)

Anonymous Referee #1

Summary:
The paper reports on an aerosol event that was observed with lidars in southwest Germany during the HOPE campaign in 2013. Over the presented period of 1 hour, the multi-parameter BASIL lidar, the key instrument in this study, measured a slowly descending, geometrically thin and stable filament of boundary-layer aerosols that exhibited diminished elastic light backscattering. This feature, which the authors dub a clear-air lidar dark band, contrasts with the prevalent dynamic conditions. With the help of wind data from a near-by wind lidar and radiosonde data it is argued that the optical phenomenon was produced by lignite particles transported from an open-pit mine about 3 km away, and that it occurred in updrafts rather than downdrafts at a background relative humidity of about 62 percent. After a short literature survey on lignite particle emissions, the authors then employ Mie theory to model the backscattering efficiency of lignite particle spectra with relatively narrow size distributions and conclude that the observed lidar dark band may be the result of the particles growing by water uptake during updrafts, with the backscattering efficiency passing through a local minimum. No satisfactory explanation is given why the reversal process likely to occur in downdrafts does not produce a similar effect.

With the support of the additional observations from BASIL and the wind lidar now introduced in the paper, an integration in the interpretation of the observed phenomena, especially of the absence of a reversal process in the downdrafts, is provided both in this response to the referee and in the revised version of the paper (see specific details on this aspect in the answers below).

The subject material falls within the scope of Atmos. Chem. Phys., and is of interest to the aerosol lidar and modeling communities. The presented experimental data are interesting, and the explanation is plausible, however, more effort should be made to better support the conclusions, especially, profiles of other parameters as measured with BASIL should be included in the study, and the origin of the observed air masses should be accessed more carefully.

We agree with the referee on the need to support the characterization and interpretation of the observed phenomenon based on the consideration in the study of the vertical profiles of other parameters measured by BASIL. In this direction, vertical profiles for a variety of additional parameters (namely, particle backscattering coefficient at 1064 nm, particle depolarization at 532 nm and relative humidity from BASIL, and wind direction from the wind lidar) in temporal coincidence with updrafts and downdrafts are now considered in the study and have been introduced in the modified version of figures included in the revised paper. The combined use of these additional information also allows to get a further confirmation of the origin of the observed air masses (see details below).

In summary, the manuscript is suited for publication in Atmos. Chem. Phys., however, revisions are deemed necessary.

We appreciate the possibility for improve the manuscript based on the precious comments and suggestions provided by the reviewer.

General comments:

1. BASIL is, according to Section 2, a high-performance multi-parameter instrument, capable of measuring water vapor, temperature, and several aerosol optical properties at up to three wavelengths, including depolarization ratio and extinction ratios. How come then that only its range-corrected backscatter signal at 1064 nm (RCS1064) and the 532-nm depolarization ratio (DR532) are used to visualize the lidar dark band? Neither the water vapor and temperature measurements are utilized to determine relative humidity directly …

The vertical profiles of water vapour mixing ratio and temperature as measured by the Raman lidar are now considered in the study to obtain independent measurements of relative humidity and its time evolution, with a specific focus on the vertical profiles in time coincidence with convective updrafts and downdrafts. Profiles of relative humidity from BASIL have been included in the revised version of figure 6 (formerly figure 5), together with the simultaneous measurements of the particle backscattering coefficient at 1064 nm, β_{1064}, and particle depolarization at 532 nm, δ_{532}, (from BASIL), and wind direction measurements (from the wind lidar).

… nor the set of particle optical properties is exploited to obtain some microphysical parameters of the aerosol as constraints for the model runs.

In the revised version of the paper some of the particle optical properties measured by BASIL are used to obtain information on aerosol microphysical parameters. Specifically, the comparison of measured and simulated values of the particle backscattering coefficient at 1064 nm allows obtaining estimates of particle number density. We have estimated a particle number density of 0.8-1.2x10^5 m^{-3} and 2.5-3.5x10^3 m^{-3} in the small (centered on 4 μm) and large (centered on 20 μm) particle domain, respectively, in agreement with the values reported by various authors (among others, Mészáros, 1991, 0.8-3.5x10^5 m^{-3} for a particle radius of 4 μm and 1-2x10^3 m^{-3} for a particle radius of 20 μm). Additionally, the determination of the backscatter color ratio, *BCR*, (specifically the ratio of total backscattering coefficients at 1064 and 532 nm) and its vertical variability (values found to decrease from 0.40-0.45 below the dark band to 0.33-0.36 within the dark band region) allowed to get an additional confirmation of the conjectured particles' growth during ascent (see more comments and the new introduced sentences below). Furthermore, the variability of the backscatter color ratio with particle radius has also been simulated and the comparison between measured and simulated values of this quantity indicates a particle size in the range 7-11 μm. Finally, a rough estimate of particle sizes is inferred by comparing measured and literature values of both color ratio and depolarization, as in fact values of *BCR* in the range 0.35-0.54 and δ_{532}<0.05 were also reported by Franke *et al.* (2003) and Müller *et al*. (2007) for Southeast Asian aerosols. These aerosols had been found to possess a pronounced coarse mode, being originated mainly from coal and dried plants used for domestic heating and cooking (Müller *et al*., 2007). Specifically, the determination of particle number concentration and radius allows to impose a constraint in our model runs. It is to be finally pointed out that despite these new results, which allow to constraint our model runs, a number of new citations of additional literature in support of our observations have been introduced (among others, Burton et al., 2012; Burton et al., 2013; Burton et al., 2014; Burton et al., 2015; Dieudonné et al., 2017; Freudenthaler, 2016; Groß, S, 2015; Mészáros, 1991;

Mona et al., 2012; Franke et al., 2003; Müller et al., 2007; Petzold, 2011; Martin, 1993; Mishchenko and Lacis, 2003; Couvreux et al., 2005, 2007; Wulfmeyer et al., 2010, 2016; Turner et al., 2014).
The following new sentences have been introduced in the text: "An additional quantity, namely the backscatter color ratio, *BCR*, i.e. the ratio of total backscattering coefficients at 1064 and 532 nm, was determined from BASIL measurements. Color ratio profiles measured during the time interval considered in the present study (12:00-13:00 UTC on 18 April 2013, not shown here) indicate values in the range 0.40-0.45 below the dark band and in the range 0.33-0.36 within the dark band region. The color ratio decrease is an indication of the increase of particle size. This represents an additional experimental evidence of the conjectured particles' growth, which represents the basis of the given interpretation of the observed phenomenon. Furthermore, small backscatter color ratio values, as those found both below and within the dark band, are indicating relatively large particles (Burton *et al*., 2013), compatible with those conjectured in the present study and presently considered in our simulations. The variability of backscatter color ratio as a function of particle radius has been simulated with the same Mie scattering code already used above, with simulations revealing that values of *BCR* in the range 0.33-0.45 are compatible with particle size in the range 7-11 μm. Finally, backscatter color ratio values in the range 0.33-0.45 combined with values of δ_{532} in the range 0.02-0.07 are in agreement with previously observed values of these quantities, as reported by a variety of authors (de Villiers *et al*., 2010, *BCR*=0.3-0.5 and δ_{532}=0.02-0.08; Burton *et al*.; 2014, *BCR*=0.55 and δ_{532}=0.07; Burton *et al*., 2015, *BCR*=0.47 and δ_{532}=0.06-0.09). Similar values (*BCR*=0.35-0.54 and δ_{532}<0.05) were also reported by by Franke *et al.* (2003) and Müller *et al*. (2007) for Southeast Asian aerosols, which were argued to possess a pronounced coarse mode, with large particles being originated mainly from coal and dried plants used for domestic heating and cooking cooking (Müller *et al*., 2007).
The comparison of simulated values of single-particle backscattering coefficient $Q_{back} \times r^2$ (~ 3×10^{-11} m^2 sr^{-1} for a particle radius of 4 μm and ~ 1×10^{-9} m^2 sr^{-1} for a particle radius of 20 μm) with measured values of the volume backscattering coefficient β_{1064} (in figures 5, in the range 2.5-3.5×10^{-6} m^{-1} sr^{-1} within the dark band) leads to an estimate of particle number density *n* of 0.8-1.2×10^5 m^{-3} and 2.5-3.5×10^3 m^{-3} in the small and large particles' domain, respectively. These values of *n* are in agreement with literature values for continental and urban polluted aerosols (among others, Mészáros, 1991, 0.8-3.5×10^5 m^{-3} for a particle radius of 4 μm and 1-2×10^3 m^{-3} for a particle radius of 20 μm)."

And why is only RCS1064 given and not the particle backscatter coefficient (PBC1064), the physically meaningful quantity?

In the revised version of the manuscript the particle backscattering coefficient is considered in substitution to the range corrected signal at 1064 nm (β_{1064}).

The reviewer understands that the measurement conditions were certainly difficult around noon, so probably water vapor and temperature may not be readily available.

As already mentioned above, vertical profiles of relative humidity, obtained from the simultaneous Raman lidar measurements of water vapor mixing ratio and temperature profiles from BASIL, have now been introduced in the revised version of figure 6 (formerly figure 5). It is to be pointed out that water vapour mixing ratio and temperature profile measurements by BASIL are based on the application of the vibrational and rotational Raman lidar technique, respectively. Both techniques rely on inelastic (Raman) backscatter phenomena, which are characterized by cross-sections that are several orders of magnitude smaller than the cross-sections characterizing the elastic backscatter phenomena. This makes water vapour mixing ratio and temperature measurements, and consequently RH measurements, very difficult to perform, especially in daytime conditions around

noon, as is the case of the measurements illustrated in this paper. This is due to the large solar irradiance affecting the Raman lidar measurements in this portion of the day. This translates into a large statistical uncertainty affecting RH measurements, and consequently large error bars in figure 6, with the random error typically ranging between 4 and 8 % in the altitude region around 1200 m where the particle backscatter minima are observed.
RH profiles measured by BASIL show very similar values in this altitude region during updraft and downdrafts. However, the presence of large statistical uncertainties, and the consequent lack of sensitivity in RH measurements, prevents from revealing any small RH variation between updraft and downdrafts, and consequently prevents from drawing any final conclusion on the motivation behind the absence of the dark-band phenomenon during down-drafts (revealing a small RH variation between updraft and downdrafts would have allowed to justify the absence during particles' descent of a particle growth reversal process, expected from the evaporation of the previously up-taken water, and would have consequently supported our interpretation of the absence of the dark-band feature during down-drafts).

But some sort of microphysical analysis and certainly calculation of PBC1064 should be possible and should be part of this investigation.

In the revised version of the manuscript the particle backscattering coefficient is considered in substitution to the range corrected signal at 1064 nm (β_{1064}). Additionally, as already mentioned above, information on specific aerosol microphysical parameters is inferred from the multi-wavelength particle backscatter and depolarization measurements. More specifically, an assessment of particle number density in both the small and large range domain is now obtained by comparing measured values of β_{1064} with simulated values of $Q_{back}*r^2$ (the latter being the new simulated quantity we are now focusing our attention following the reviewer's suggestion). This comparison allowed to obtained estimates of particle number density: we estimated a particle number density of 0.8-1.2x10^5 m^{-3} and 2.5-3.5x10^3 m^{-3} in the small (centered on 4 μm) and large (centered on 20 μm) particle domain, respectively. These estimated values are found to be in agreement with those reported by various authors (among others, Mészáros, 1991, 0.8-3.5x10^5 m^{-3} for a particle radius of 4 μm and 1-2x10^3 m^{-3} for a particle radius of 20 μm). Additionally, we also determined the color ratio, i.e. the ratio of the total backscattering coefficients at 1064 and 532 nm (β_{1064}/β_{532}). This quantity is known to be dependent of particle size, with a tendency to increase with decreasing particle size. The color ratio is found to have values in the range 0.40-0.45 below the dark band and in the range 0.33-0.36 within the dark band region., i.e. within the same region where the β_{1064} reduction of ~ 10 % is observed. This decrease in color ratio indicates an increase of particle size during its uplift. Thus, an additional experimental evidence of the particles' growth conjectured in the interpretation of the observed phenomenon is provided. The text has been modified and integrated with the introduction of the following sentences/paragraphs.
"An additional quantity, namely the backscatter color ratio, *BCR*, i.e. the ratio of total backscattering coefficients at 1064 and 532 nm, was determined from BASIL measurements. Color ratio profiles measured during the time interval considered in the present study (12:00-13:00 UTC on 18 April 2013, not shown here) indicate values in the range 0.40-0.45 below the dark band and in the range 0.33-0.36 within the dark band region. The color ratio decrease is an indication of the increase of particle size. This represents an additional experimental evidence of the conjectured particles' growth, which represents the basis of the given interpretation of the observed phenomenon. Furthermore, small backscatter color ratio values, as those found both below and within the dark band, are indicating relatively large particles (Burton *et al*., 2013), compatible with those conjectured in the present study and presently considered in our simulations. The variability of backscatter color ratio as a function of particle radius has been simulated with the same Mie scattering code already used above, with simulations revealing that values of *BCR* in the range 0.33-0.45 are compatible with particle size in the range 7-11 μm. Finally, backscatter color ratio values

in the range 0.33-0.45 combined with values of δ_{532} in the range 0.02-0.07 are in agreement with previously observed values of these quantities as reported by a variety of authors (de Villiers *et al*., 2010, *BCR*=0.3-0.5 and δ_{532}=0.02-0.08; Burton *et al*.; 2014, *BCR*=0.55 and δ_{532}=0.07; Burton *et al*., 2015, *BCR*=0.47 and δ_{532}=0.06-0.09). Similar values (*BCR*=0.35-0.54 and δ_{532}<0.05) were also reported by Franke *et al.* (2003) and Müller *et al*. (2007) for Southeast Asian aerosols, which were argued to possess a pronounced coarse mode, with large particles being originated mainly from coal and dried plants used for domestic heating and cooking (Müller *et al*., 2007).
The comparison of simulated values of single-particle backscattering coefficient $Q_{back} \times r^2$ (~ 3×10^{-11} m^2 sr^{-1} for a particle radius of 4 μm and ~ 1×10^{-9} m^2 sr^{-1} for a particle radius of 20 μm) with measured values of the volume backscattering coefficient β_{1064} (in figures 5, in the range 2.5-3.5×10^{-6} m^{-1} sr^{-1} within the dark band) leads to an estimate of particle number density *n* of 0.8-1.2×10^5 m^{-3} and 2.5-3.5×10^3 m^{-3} in the small and large particles' domain, respectively. These values of *n* are in agreement with literature values for continental and urban polluted aerosols (among others, Mészáros, 1991, 0.8-3.5×10^5 m^{-3} for a particle radius of 4 μm and 1-2×10^3 m^{-3} for a particle radius of 20 μm)."
For the purpose of illustrating the results in a more coherent way, former figure 6 (now figure 5), illustrating the time–height cross-section of the particle depolarization ratio at 532 nm, δ_{532}, is now preceding former figure 5 (now figure 6). The text associated with the illustration of new figure 5 and the description of the time–height evolution of δ_{532} has been slightly modified to account for the refined calculation and calibration of δ_{532} measurements. In fact, as a results of the more quantitative assessment of the lidar observations requested by the referee, we refined the calculation and calibration of δ_{532} measurements, obtaining slightly smaller values for this quantity. Now, δ_{532} ranges from values of 0.05-0.07 below the dark band to values of 0.02-0.03 within and above the dark band. In section 3, after the sentence ending with "respectively (Di Girolamo *et al*., 2012a)", the following sentences have been introduced: "Figure 5 reveals a decrease in particle depolarization at the same height and time intervals of the dark band. More specifically, δ_{532} decreases from values of 0.05-0.07 below the dark band to values of 0.02-0.03 within and above the dark band. A decrease of δ_{532} within and above the dark band is compatible with the conjectured size growth of the uplifted dry lignite particles, initially having a more irregular shape, and then getting a more regular spherical shape as a result of the water uptake. Additionally, as previously observed for β_{1064}, the decrease of δ_{532} occurs during up-drafts, but not during down-drafts, as in fact during these latter values of δ_{532} are in the range 0.02-0.04 both below and within the dark band. However, both below and within the dark band values of δ_{532} are rather low, which is typical of aerosols including a large portion of carbonaceous species as those resulting from fossil fuel combustion, having a rather spherical shape (Dieudonné *et al*., 2017; Müller *et al*., 2007). Particle depolarization ratio measurements, while providing some information on particle shape, may also be used for aerosol typing and mass concentration studies (among others, Petzold, 2011; Burton *et al*., 2012)."

2. Because DR532 is significant, application of Mie theory is questionable. Please, discuss.

As requested by the referee, we performed a more quantitative assessment of the lidar observations trying to go beyond the more qualitative one originally provided in the first version of their paper. As a result of this integration of analysis, we have now refined the calculation and calibration of DR532 measurements (δ_{532} in the text), obtaining slightly smaller values for this quantity. Now, δ_{532} ranges from values of 0.05-0.07 below the dark band to values of 0.02-0.03 within and above the dark band, while before the refinement of the calculation and calibration δ_{532} was ranging from values of 0.30-0.35 below the dark band to values of 0.15-0.20 within and above the dark band. We believe that when dealing with these smaller values of δ_{532} the application of the Mie theory in the interpretation of the results is less questionable. Nevertheless, the applicability of the Mie theory in

the presence of slightly non-spherical particles is now discussed in the paper. More specifically, we are now clearly pointing out that Mie theory can still be applied for particles characterized by a limited degree of asphericity (Martin, 1993; Mishchenko and Lacis, 2003). In this regard, the following sentence has been introduced in section 4, when illustrating the simulations and their results: "In this respect it is to be specified that the small values of δ_{532} characterizing the observed aerosol particles call for a very limited degree of asphericity, which makes Mie theory still successfully applicable for the simulation of particles' scattering properties (Martin, 1993; Mishchenko and Lacis, 2003)."

3. Discussion on Figs. 7 and 8, page 6: Why is backscattering efficiency in arbitrary units, and why is backscattering efficiency presented at all?

The referee is write. There was a misprint as in fact the backscattering efficiency was supposed to be expressed in sr^{-1}. However, backscattering efficiency (Q_{back}) is no longer illustrated in figure 7, having been replaced from the quantity $Q_{back}*r^2$, as suggested by the referee. This is now the quantity compared to measured values of β_{1064}.

Assuming a constant particle number density n, particle backscatter coefficient is proportional to the product of backscattering efficiency Q and the square of the particle radius, rˆ2. So, Qrˆ2 should be modeled to explain the lidar dark band, and ideally it should be compared to the BASIL measurements of PBC1064.

As suggested by the referee, we are now modeling the quantity $Q_{back}*r^2$, which is the quantity now visualized in figure 7. We are now using this quantity also for the interpretation of the observed lidar dark band phenomenon and comparing this quantity to BASIL measurements of β_{1064}. In this regard, the corresponding text in section 4 of the paper has been changed as follows: "Simulations of the scattering properties of lignite particles are illustrated in figure 7. The figure shows the variability of the quantity $Q_{back}{\times}r^2$ as a function of r, with Q_{back}, being the backscattering efficiency and r being the particle radius." …. "The quantity $Q_{back}{\times}r^2$ represents the single-particle backscattering coefficient, assuming a constant particle number density n." … "The comparison of simulated values of single-particle backscattering coefficient $Q_{back}{\times}r^2$ (~ $3x10^{-11}$ m^2 sr^{-1} for a particle radius of 4 μm and ~ $1x10^{-9}$ m^2 sr^{-1} for a particle radius of 20 μm) with measured values of the volume backscattering coefficient β_{1064} (in figures 5, in the range 2.5-3.5$x10^{-6}$ m^{-1} sr^{-1} within the dark band) leads to an estimate of particle number density n of 0.8-1.2$x10^5$ m^{-3} and 2.5-3.5$x10^3$ m^{-3} in the small and large particles' domain, respectively. These values of n are in agreement with literature values for continental and urban polluted aerosols (among others, Mészáros, 1991, 0.8-3.5$x10^5$ m^{-3} for a particle radius of 4 μm and 1-2$x10^3$ m^{-3} for a particle radius of 20 μm)."

Note that a decrease in Q of 10% (top panel) and 40% (bottom panel) as modeled maximally for small and large initial lignite particles (Fig. 7) would be compensated for by an increase in r by a factor of 1.05 and 1.19, respectively.

Authors are not sure to understand the point made by the referee here as in fact it is this "compensation" of the decrease in Q_{back} with an increase of the particle radius (i.e. particle growth process) that we are referring to with the purpose of interpreting the observed phenomena. In the previous version of the paper, former figure 7 was showing a decrease in Q_{back} by ~ 15 % for small initial lignite particles (top panel) and by ~ 40% for large initial lignite particles (bottom panel), which could be caused by an increase of particles' radius r by ~ 15 and 30 %, respectively. More specifically, Q_{back} had been modeled (upper portion of the former version of figure 7) to be equal to 1,565 for r = 2,62 μm and equal to 1,364 for r = 2,99 μm, which corresponds to a decrease in Q_{back} of 13 % associated with an increase of the radius r by 14 %; analogously, Q_{back} had been modeled

(lower portion of the former version of figure 7) to be equal to 4,2 for r = 16,3 μm and equal to 2,3 for r = 21,4 μm, which corresponds to a decrease in Q_{back} of 45 % associated with an increase of the radius r by 31 %; furthermore, Q_{back} was found (former version of figure 7, lower portion) to be equal to 6,1 for r = 27,8 μm and equal to 3,9 for r = 33,0 μm, which corresponds to a decrease in Q_{back} of 36 % for an increase of the radius r by 19 %. This result had been included in the former version of the paper with the sentence: "As a result of these oscillations, for specific radius values of the dry lignite particles (for example, 6.5 μm, 7.5 μm, 18 μm, 28.5 μm, 41 μm), a reduction in Q_{back}*r^2 of 8-27 % (0.35-1.4 dB) is observed for a particle size growth by 10-16 %, which is the size growth experienced by these particles during their adiabatic ascent".
The former considerations of the variability of the quantity Q_{back} as a function of the particle radius r are now confirmed and substantiated by the consideration of the quantity Q_{back}*r^2, which is the quantity now included in figure 7. Specifically, Q_{back}*r^2 is found to decrease (upper portion of new figure 7) from an initial value of 9.5x10^{-11} m^2 sr^{-1} for r = 7.5 μm to a value of 8.8x10^{-11} m^2 sr^{-1} for r = 8,4 μm, which corresponds to a decrease in Q_{back} of 8 % for an increase of the radius r by 12 %; analogously, Q_{back}*r^2 is found to decrease (lower portion of the new version of figure 7) from an initial value of 5.2x10^{-11} m^2 sr^{-1} for r = 28,5 μm to a value of 3.8x10^{-11} m^2 sr^{-1} for r = 33,0 μm, which corresponds to a decrease in Q_{back} of 27 % for an increase of the radius r by 16 %; finally, Q_{back}*r^2 is found to decrease (lower portion of the new version of figure 7) from an initial value of 1.28x10^{-8} m^2 sr^{-1} for r = 41 μm to a value of 1.05x10^{-8} m^2 sr^{-1} for r = 45 μm, which corresponds to a decrease in Q_{back} of 28 % for an increase of the radius r by 10 %.

4. According to Figs. 3 and 4, westerly winds (> 240 degrees wind direction) prevailed throughout the boundary layer which did not pass over the open-pit mine (Fig. 1). The only exception is the dark-band layer characterized by slightly more southerly winds blowing from the edge of the pit. So isn't it possible that BASIL simply observed air masses of different origin (and therefore different aerosols) at different heights?

The point is that the dark-band is observed during updrafts and not during downdrafts, bearing in mind the shown evident correlation between the presence of the backscatter minimum and the strong positive vertical wind speeds (updrafts) and between the absence of the backscattering minimum and the strong negative vertical wind speeds (downdrafts). This correlation is even more clear in the new version of figures 2, 4 and 5, that we generated following the suggestions of the referee. In this direction, the modified version of figure 6 (formerly figure 5) is very emblematic, as in fact no evidence of a wind direction change is observed when passing from periods with to periods without the dark band. Additionally, again following the requests of the referee, the layout of figure 4 has been improved with the introduction of colored curves and the use of a narrower direction range (180-320 degrees). This new version of figure 4 now clearly reveals that the average wind direction over the time interval 12:00-13:00 UTC on 18 April 2013, i.e. the time interval we are focusing our attention in this paper, has values in the range 230-240 degrees throughout the vertical interval 800-1350 m, which testify the presence of winds blowing from the open-pit mine. A 1h average wind direction profile with values in the range 230-240 degrees reveals that indeed this wind direction was not sporadically experienced during the observation period.
Additionally, what appears quite anomalous here - and calls for a non-dynamical interpretation of the observed phenomenon - is the fact that the region of reduced backscattering persists at an almost fixed height albeit the evident presence of up-drafts and down-drafts, which should have at least perturbed its shape. So, instead of having a time-height cross-section of β_{1064} with the dark band appearing as a straight horizontal line feature, in case of a prevailing dynamical cause an alternating structure should be present. Finally, the presence of alternating intensity fluctuations, with the backscatter minimum occurring during up-drafts, but not during down-drafts, would be difficult to explain when considering different aerosol types at different altitudes.

Or asked differently, how certain can one be that really aerosol growth was observed? Please, discuss.

We believe that here the observation of an aerosol growth process is quite likely, but it is obviously not certain. This aspect has been more clearly addressed in the text of the paper with the consideration of a more prudential interpretation of the results and with the introduction in the section "Summary and final remarks" of the following sentence: "Observations and results illustrated in this paper support the interpretation of the phenomenon as a purely microphysical growth mechanism; however, the possibility that other mechanisms (for example, dynamics) may also participate and contribute to the appearance of the phenomenon cannot be completely excluded."

5. Page 7, lines 29ff., page 8, lines 27ff.: In their discussion of the differing aerosol behavior in up- and downdrafts the authors mention the possibility that different particles were measured. The reviewer agrees, see 4. (above). To investigate this important issue, the authors should not only show vertical wind speed for up- and downdraft periods in Fig. 5 but also wind direction.

As suggested by the referee, we integrated the investigation of this issue with the introduction in the modified version of figure 6 (former figure 5) of the wind direction measurements for updrafts (panels a, c, e, g) and downdraft periods (panels b, d, f, h). As additionally suggested by the referee, the vertical wind speed (from the wind lidar) is now illustrated together with the simultaneous measurements of the particle backscattering coefficient at 1064 nm, β_{1064}, and particle depolarization at 532 nm, δ_{532}, (from BASIL) and vertical wind speed measurements (from the wind lidar). Wind direction profiles in this figure very emblematically reveal that no evidence of a wind direction change is observed when passing from periods with the dark band to periods without the dark band.
In our discussion of the results the possibility that "down-drafts transport other or modified particles than the up-drafts" is considered. However, in this discussion we are primarily referring to the possibility of having entrainment of air from the free troposphere. This is now more clearly specified in the paper, where the text has been changed as follows: "The possibility that particles within the down-drafts are different from those within the up-drafts increases in the interfacial layer due to the entrainment effects and is possibly testified by the presence of smaller particle backscatter values within the down-drafts with respect to those observed within the up-drafts (see figure 2). This is possibly associated with the entrainment of air from the free-troposphere at the top of the CBL, which may ultimately lead to changes in particle size distribution and scattering properties. Evidence of the sharp entrainment of air pockets from the free troposphere into the boundary layer, which gradually mix with the environmental air, has been reported by a variety of authors (Couvreux et al., 2005, 2007; Wulfmeyer et al., 2010, 2016; Turner et al., 2014). Particle size distribution within the down-draft could be not as narrow as in the updrafts, resulting in a smear out of backscatter efficiency oscillations."

Specific comments:

1. Page 3, lines 29, 30: Please, discard RCS1064 in Fig. 3 and show the full profile of PBC1064 instead for a better understanding of the measurement situation.

The particle backscattering coefficient at 1064 nm is now plotted instead of the original range-corrected signal. The full profile of this quantity is now included in the plot.

2. Page 4, line 25: This is no true. Depolarization ratio also depends on size and refractive index of the aerosol particles. Please, be more accurate.

The reviewer is right in underlining that particle depolarization depends not only on the degree of asphericity of sounded aerosol particles, but also on their size and refractive index. The sentence here has been reformulated in order to make it more accurate and now reads: "Particle depolarization ratio, defined as the power ratio of the cross-polarized to the co-polarized components of the particle backscattering coefficient, provides an indication of the degree of asphericity of sounded particles". Additionally, the following new sentence has been introduced: "Particle depolarization depends not only on particles' shape, but also on their size and refractive index (among other, Burton *et al*., 2015)."

3. Page 5, line 1: The authors probably mean 'Figure 6'. The observation made is not at all obvious. Please, show some example profile pairs (PBC1064, DR532).

Indeed in the text we are referring to figure 6 and not to figure 7. In the new version of this figure (now figure 5) we are now considering a clearer color scale for DR532 in order to make the variability of this quantity easier to reveal and the observations reported in the text more obvious. Besides that, the vertical profiles of PBC1064 (β_{1064}) and DR532 (δ_{532}) have now been introduced in the new version of figure 6 (formerly figure 5) in order to underline the anti-correlated behavior characterizing the vertical variability of these two quantities.

4. Page 6, line 4: How do the authors arrive at the conclusion of 15-30% size growth? And is it volume, mass, diameter growth?

We assume that lignite particles advected by the wind to the lidar site are captured and ingested within the updrafts and downdrafts associated with the intensive convective activity present at the lidar site. As a result of the adiabatic cooling associated with the uplift, air-parcels undergo a sudden RH increase from values in the range 60-62 % (environmental RH values at the base of the dark band) to values in the range 75-80 % (these latter being the values reached within the lifting air-parcel assuming an ideal adiabatic cooling with no air entrainment into the convective plumes or external air ingestion within the lifting air-parcel).
The solution effect is well known to typically dominate hygroscopic particles' growth when the radius is smaller than the critical radius, which results in small solution droplets being in equilibrium with water vapour at RH values less than 100 %. At this stage, small increases in RH determine particles' size growth until equilibrium is newly reached, i.e. if relative humidity increases by a small amount, the solution droplet grows until equilibrium is reached again. The change in radius associated with a certain variation in relative humidity can be quantified based on the application of the Köhler equation, which is dominated by the solution term when RH values are smaller than 100 %. This term depends on the mass and molecular weight of the solute species and the so called van't Hoff factor. Based on literature values of these quantities, an increase in RH from 60-62 to 75-80 % is expected to determine particles' size growth in radius by 10-20 %. Such percentage increase in particle radius is compatible with the simulated particle radius growth (10-16 %) capable to determine the observed percentage reduction in the backscattering coefficient (~10 %). This aspects are now better clarified in the text. Specifically, when describing the relative humidity change experienced by the aerosol particles during their uplift, the following sentences have been introduced: "At this stage, small increases in RH determine particles' size growth until equilibrium is newly reached. This mechanism is possibly responsible for the lignite particle growth below the LCL, ultimately leading to the appearance of a minimum in lidar backscatter echoes (i.e. the above mentioned clear-air dark band phenomenon). The increase in particles' radius associated with the relative humidity change experienced by the adiabatically uplifted air-parcel can be estimated based on the application of the Köhler equation. When RH values are smaller than 100 %, the Köhler equation is dominated by the solution term, which depends on the mass and molecular

weight of the solute species and the so called van't Hoff factor. Based on literature values of these quantities, the above specified increase of RH from 60-62 to 75-80 % would result in a particle size growth in radius by 10-20 %."

Figures:

All figures: Use the same style, make sure axis labels and titles are easy to read.

We have improved the layout of all figures in the direction suggested by the referee. Now the same style is used in all figures. We also modified the axis labels and titles of several figures in order to make them easier to read.

Figure 2, upper panel: Show PBC1064. Dotted line hard to see. Color bar?

The dotted line in the upper portion of figure 2 has been made thicker in order to make it easier to see. Here the particle backscattering coefficient at 1064 nm is now plotted instead of the original range-corrected signal. The color bar was missing in the upper portion of figure 2 and has now been introduced.

Figure 2, lower panel: Up-/down drafts hardly visible, use different color table.

As suggested by the referee, the color scale has been changed in order to make updrafts and downdrafts easier to see. In this direction, a smaller vertical velocity range has been considered (formerly ± 5, now ± 3), as well as a larger number of colors in the color table.

Figure 3: Show PBC1064, full profile.

The full profile of the particle backscattering coefficient at 1064 nm is now illustrated in figure 3.

Figure 4: Use colored curves instead of symbols, explain curves in caption. Choose narrower direction range so that relevant values can be better judged, for instance 180-320 degrees.

Figure 4 has been changed in the direction suggested by the reviewer. Colored curves are now used instead of symbols. A narrower direction range has been considered in order to make relevant values easier to judge (we are now considering the direction range 180-320 degrees instead of the original 0-360 degrees). All profiles are now explained in the figure caption, which now reads: "Vertical profile of wind speed and direction averaged over the time interval 12:00-13:00 UTC on 18 April 2013 as measured by the wind lidar located in the proximity of BASIL at the Supersite JOYCE. Profiles are reported with error bars, corresponding to ± 1 standard deviation." Finally, the figure was also simplified with the removal of two profiles, representing the minimum and maximum wind speed and direction, which were probably not necessary and overloading the figure.

Figure 5: Good start. Please, show PBC1064 instead of RCS1064. Also include DR532 and wind direction for a better characterization of the particles and the measurement conditions, respectively.

Figure 5 (now renamed figure 6) has been changed and now includes PBC1064 (β_{1064}) instead of RCS1064. Additionally, in this figure we are now including the vertical profile of particle depolarization at 532 nm (δ_{532}) and wind direction. The inclusion of δ_{532} in figure 5 imposed some reshuffling of the text. In fact, in the original version of the paper the quantity δ_{532} had been introduced in figure 6, which was representing the time–height cross-section of δ_{532} over the same

time interval considered in figure 2 (i.e. 12:00-13:00 UTC on 18 April 2013). The consideration of δ_{532} in former figure 5 (now figure 6) imposes that former figure 6 (now figure 5) is moved ahead.

Figure 6: As previously noted, it is hard to discern (anti)correlations comparing Figs. 2 and 6 by eye. Example profile pairs (PBC1064, DR532) would help.

In figure 2 and 5 (formerly 6) we are now considering a clearer color scale for PBC1064 (β_{1064}) and DR532 (δ_{532}), respectively, in order to make their variability easier to reveal. Besides that, as suggested by the referee, the vertical profiles of β_{1064} and δ_{532} have been introduced in figure 6 (formerly figure 5) in order to easily reveal the anti-correlations characterizing the vertical variability of these two quantities.

Technical corrections:

1. Throughout text: Subscripts that are not variables must not be italic

Subscripts have been corrected throughout the text.

2. Abstract, 1st line: Remove ‘)’at line end

Corrected.

3. Page 1, line 17: ‘200 m’

Corrected.

4. Page 2, line 8: ‘for a selected’

Corrected.

5. Page 3, line 25: ‘on other days’

Corrected.

6. Page 4, line 8: ‘wind to the’

Corrected.

7. Reference Civis… : Remove ‘Jan’

Corrected.

8. Reference Krawczy… : Include ‘and’ between authors.

Corrected.

9. Reference Yau… : Include ‘and’ between authors, move to end of list

Corrected.

Anonymous Referee #2

General Comments

This paper is very well written and deals with a unique lidar aerosol observation. The case is made for subtle growth by condensation of water on a narrow size distribution of aerosol. Under very specific atmospheric conditions the growth can result in a Mie backscatter minimum at a certain altitude. The lidar and radiosonde data are brought together to make a consistent argument for being able to see this occurrence. This paper is appropriate for ACP and can be published with minor corrections.

We are very pleased for the positive words expressed by the referee. We also appreciate the possibility for further improve the manuscript based on his precious suggestions.

Specific comments

Abstract: no comments

Page 2: Line 23: These eleven detected signals allow(s) determining …

Corrected.

Page 3: Line 15: This minimum persist(s) albeit …

Corrected.

Page 5: Line 1: Figure 7 reveals … Shouldn't that be Figure 6?

The referee is right. This misprint has now been corrected in the revised version of the paper. However, figure 6 has been renamed figure 5 in the new version of the paper.

Figure 7: end of caption: 1.064 micrometers not millimeters

Corrected.

Anonymous Referee #3

Summary:

This paper presents an interesting case study of multiwavelength lidar measurements (including linear depolarization ratio measurements) of an unusual aerosol event made during the HOPE campaign in 2013. A thin layer of boundary layer aerosol with an apparently distinctly low associated backscatter coefficient was observed giving rise to a "clear-air dark band". The authors discuss the measurements and offer an explanation for the observations. Namely, they hypothesis that the layer was produced by hydrating lignite particles from a local open-pit mine.
In the main, the paper is clear, the measurements appear sound and the offered explanation seems plausible. The paper is suitable for ACP. However, there are a few areas that should be addressed before publication.

We appreciate the possibility for further improve the manuscript based on the referee's precious suggestions.

While preparing my review I have noticed that Anonymous Reviewer #1 has posted their review, which seems thorough. In the interest of efficiency (and the coming holidays) I will frame my review with reference to Reviewer #1s' comments.

General comments:
I can state that I agree with the general comments of Reviewer#1 with the exception of the contention that "No satisfactory explanation is given why the reversal process likely to occur in downdrafts does not produce a similar effect". I find that the discussion offered in the Section 5 of the paper is plausible and "complete enough" in the context of the present work. Perhaps the authors can state that this is a preliminary hypothesis and outline what exact work would be needed to test their offered explanation in a quantitative manner.

The authors agree that the discussion and interpretation of the results given in the Section 5 was plausible and "complete enough" for the purposes of this paper, whose aim was providing evidence of the observed phenomenon and illustrate possible preliminary explanations for its occurrence. However, the invitation from referee # 1 to integrate the presentation and interpretation of the results offered us the possibility to further investigate the observed phenomena and the issue of the absent reversal process in downdrafts. In this regard, the vertical profiles of relative humidity (RH) from BASIL have been included in the revised version of figure 6 (formerly figure 5), together with the simultaneous measurements of the particle backscattering coefficient at 1064 nm, β_{1064}, and particle depolarization at 532 nm, δ_{532}, (from BASIL) and wind direction and vertical wind speed measurements (from the wind lidar). RH values observed by BASIL in this altitude region are found to be very similar during updraft and downdrafts. This new version of the figure provides additional evidence of the correlated appearance of backscatter minima (dark band) in coincidence of strong updrafts (positive vertical velocity values) and the disappearance of these backscatter minima in coincidence of strong downdrafts (negative vertical velocity values). Concerning the RH measurements, it is to be pointed out that these are affected by large uncertainties. The lack of sensitivity in RH measurements prevents from revealing any small RH difference between updraft and downdrafts, and consequently prevents from drawing any final conclusion on the presence of a RH change, which could justify the absence during particles' descent of a particle growth reversal process, expected for the evaporation of the previously up-taken water, and could consequently motivate the absence during down-drafts of a dark-band feature. Additionally, the following modified text has been introduced in the discussion of the missing reversal process during downdrafts: "The possibility that particles within the down-drafts are different from those within

the up-drafts increases in the interfacial layer due to the entrainment effects and is possibly testified by the presence of smaller particle backscatter values within the down-drafts with respect to those observed within the up-drafts (see figure 2). This is possibly associated with the entrainment of air from the free-troposphere at the top of the CBL, which may ultimately lead to changes in particle size distribution and scattering properties. Evidence of the sharp entrainment of air pockets from the free troposphere into the boundary layer, which gradually mix with the environmental air, has been reported by a variety of authors (Couvreux et al., 2005, 2007; Wulfmeyer et al., 2010, 2016; Turner et al., 2014)."

I can also state that I especially agree with Reviewer#1 that the Figures need to be, in general, improved.

Following the suggestion of both referee # 1 and 3, the layout of all figures has been improved and we are now using the same style for all of them. We also modified the axis labels and titles of several figures in order to make them easier to read.

Specific Additional Comment

-Line 30 on Page 4 refers to Figure 6: I think this should be Figure 5 OR the authors have left a figure out by mistake. The discussion makes me think they are referring to a line-plot of the depolarization ratio vs height. If this is not the case, and they are really mean to be referencing Figure 5, then they should consider inserting a line plot of the depolarization. In any case, Figure 5 is not clear enough for me to draw any quantitative information from !

The sentence in line 30 of Page 4 (*"However, accurate measurements of these quantities (i.e. the cross- and co-polarized components of the particle backscattering coefficient) may be difficult to obtain, often as a result of the depolarizing properties of different optical devices included in the receiver (Freudenthaler, 2017)"*) refers to former figure 6 (now figure 5), which is the figure illustrating the time-height cross-section of particle depolarization at 532 nm. We don't understand why the referee thinks this sentence should refer to former figure 5 (now figure 6), which is instead illustrating the vertical profiles of the particle backscattering coefficient at 1064 nm (β_{1064}), formerly the range-corrected backscatter signal at 1064 nm (RCS_{1064}), and the vertical wind speed. However, a line-plot of the depolarization ratio vs height has now been introduced in former figure 5 (now figure 6), together with the vertical profiles of the particle backscattering coefficient at 1064 nm, relative humidity, wind direction and vertical wind speed. We have the impression that the statement "*Figure 5 is not clear enough for me to draw any quantitative information from*" by the referee is intended to refer to former figure 6 (now figure 5) and not former figure 5 (now figure 6) as in fact former figure 6 figure was a color map illustrating the time-height variability of particle depolarization without a clear color scale and this was making very difficult to properly infer the values of this quantity, while former figure 5 was illustrating the vertical profiles of several quantities (range corrected signal at 1064 nm, vertical wind velocity, now also particle backscattering coefficient at 1064 nm, relative humidity and wind direction) from which quantitative information could be easily drawn. Nevertheless, we sensitively improved the layout of both figures so that now quantitative information can be easily drawn.

Clear-air lidar dark band

Paolo Di Girolamo[1], Andrea Scoccione[2], Marco Cacciani[2], Donato Summa[1], Benedetto De Rosa[1], Jan H. Schween[3]

[1]Scuola di Ingegneria, Università degli Studi della Basilicata, Italy
[2]Dipartimento di Fisica, Università di Roma "La Sapienza", Italy
[3]Institut fuer Geophysik und Meteorologie, Universität zu Köln, Germany

Correspondence to: Paolo Di Girolamo (digirolamo@unibas.it)

Abstract. This paper illustrates measurements carried out by the Raman lidar BASIL in the frame of the HD(CP)2~~)~~ Observational Prototype Experiment (HOPE), revealing the presence of a clear-air dark band phenomenon (i.e. a minimum in lidar backscatter echoes) in the upper portion of the convective boundary layer. The phenomenon is clearly distinguishable in the lidar backscatter echoes at 532 and 1064 nm, as well as in the particle depolarization data. This phenomenon is attributed to the presence of lignite aerosol particles advected from the surrounding open pit mines in the vicinity of the measuring site. The paper provides evidence of the phenomenon and illustrates possible interpretations for its occurrence.

1 Introduction

In the frame of the HD(CP)2 Observational Prototype Experiment (HOPE), the Raman lidar system BASIL was deployed and operated over a two-month period (April-May 2013) in the Atmospheric Supersite JOYCE, located within the Jülich Research Centre. This site is approximately 3 km West of the *Tagebau-Hambach* open-pit lignite mine, which represents the largest operational lignite mine on Earth, with a maximum depth of ~ 200 m (Figure 1). The dump of this mine forms a large artificial hill, called *Sophienhöhe*, which reaches 302 m and is partially re-cultivated with forest. A second open-pit lignite mine, named *Tagebau Inden*, is located approximately 3 km South-West of the Supersite.

The *Hambach* and *Inden* mines lie in the sectors 29-114° (red shaded area in figure 1) and 180-240° (blue shaded area in figure 1), respectively, relative to the location of the Raman lidar. When wind blows from these directions, lignite particles from the two open-pit mines or the surrounding hill are lifted up from the ground and transported over the lidar site, with appreciable effects on the measurements.

Evidence of this particle transportation was found in lidar elastic backscatter echoes in a variety of case studies during HOPE, with the appearance of a specific odd feature in the upper portion of the convective boundary layer (CBL). Specifically, a minimum in lidar backscatter echoes at 532 and 1064 nm, with a backscatter reduction of approximately ~~1 dB (~ 20~~ 10 %~~),~~ is observed. This feature is found to have a vertical extent of approximately 100 m and persist over a period of several hours, with an alternation of intensifications and attenuations of the phenomenon. Similar features with a comparable temporal duration and backscatter reduction had been reported by Sassen and Chen (1995) in the presence of light

precipitation events; this phenomenon, referred to as *lidar dark band*, was demonstrated to be ascribable to changes in scattering properties of precipitating particles taking place during the snowflake-to-raindrop transition in the proximity of the melting level (Sassen *et al*., 2005; Demoz *et al*., 2000; Di Girolamo *et al*., 2003; Di Girolamo *et al*., 2012b).

Instead, the phenomenon reported in the present research effort appears in clear-air conditions and in the presence of strong convective activity within the boundary layer: we will refer to it in the following as the clear-air dark band phenomenon or the convective dark band phenomenon. In the following of this paper we provide experimental evidence of this phenomenon and a possible physical interpretation for its occurrence.

The outline of the paper is the following. Section 2 provides a description of the experimental set-up and a brief overview of the HOPE field campaign. Section 3 illustrates the measurements collected for a selected case study, providing remarks on the meteorological conditions occurring during these periods. Section 4 illustrates the hygroscopic and scattering properties of the sounded particles, while section 5 formulates possible hypotheses for the interpretation of the observed phenomena. Finally, section 6 summarizes all results and provides some indications for possible future measurements and analysis.

2 BASIL and the HOPE field campaign

The University of Basilicata Raman lidar system (BASIL) is a ground-based Raman lidar hosted in a transportable sea-tainer. BASIL performs high-resolution and accurate measurements of the vertical profiles of atmospheric temperature and water vapour, both in the daytime and at night-time, exploiting both the rotational and vibrational Raman lidar techniques in the UV (Di Girolamo *et al*., 2004, 2006, 2009a, 2016, Bhawar *et al*., 2011). Besides temperature and water vapour, BASIL also measures the vertical profiles of particle backscatter at 354.7, 532 and 1064 nm, particle extinction and depolarization at 354.7 and 532 nm (Griaznov *et al*., 2007; Di Girolamo *et al*., 2009b, 2012a, b). BASIL makes use of a Nd:YAG laser source, equipped with second and third harmonic generation crystals, which emits pulses at 354.7, 532 and 1064 nm. The receiver is built around a large aperture Newtonian telescope (primary mirror diameter: 0.45 m, focal length: 2.1 m) and two small-aperture telescopes (50mm diameter lenses). The large aperture receiver incorporates eight channels for the detection of eight different signals (primarily Raman lidar signals), while the two small-aperture receivers include another three measurement channels for the detection of additional lidar signals. These eleven detected signals allows determining the atmospheric variables listed above, plus additional ancillary parameters as the atmospheric boundary layer depth and the geometric (cloud base and top height, the latter in case of optically thin clouds) and optical (cloud optical depth for optically thin clouds) properties of clouds. More details on the experimental set-up of the system are provided in Di Girolamo *et al*. (2009a, 2017).

In this paper we illustrate measurements carried out in the frame of the High-Definition Clouds and Precipitation for advancing Climate Prediction (HD(CP)2) Observational Prototype Experiment (HOPE, Macke *et al*., 2017). For the purposes of HOPE, BASIL was deployed in the Supersite JOYCE, located within the Jülich Research Centre (Central Germany, Lat.: 50°54’ N; Long.: 6°24’ E, Elev. 105 m). The system operated between 25 March and 31 May 2013, collecting more than 430 h of measurements distributed over 44 days and 18 Intensive Operation Periods (IOPs).

3 Results

The weather at the lidar site in Jülich on 18 April 2013 was characterized by the presence of clear sky conditions in the morning until 06 UTC and by the passage of a cold front shortly afterwards. The passage of the cold front was followed by a circulation change from a south-westerly to west/north-westly marine flow, with the sky clearing up in the late morning and the onset of a strong convective activity. Boundary layer clouds were found to form in the late morning and early afternoon, while broken cirrus clouds were observed throughout the day.

Figure 2 illustrates the time–height cross-section of the ~~range corrected backscatter signal~~particle backscattering coefficient at 1064 nm, β~~*RCS*~~$_{1064}$, as measured by BASIL (upper panel), and the vertical wind speed, as measured by the University of Cologne wind lidar (lower panel), in the time interval 12:00-13:00 UTC on 18 April 2013. For the purpose of these measurements, the two lidars were located within a distance of ~ 80 m. The upper panel of the figure clearly reveals the presence of a significant aerosol loading within the boundary layer, which is tracing the presence of a well-mixed and quasi-stationary CBL at this time of the day, extending up to approximately 2000 m. The figure also reveals the presence of alternating updrafts and downdrafts. The largest variability of β~~*RCS*~~$_{1064}$ is observed in the interfacial layer, as a result of the penetration of aerosol-rich air rising from the ground and the entrainment of aerosol-poor air sinking from the free troposphere.

A persistent minimum in lidar backscatter is observed around 1200 m (black dashed line), with alternating intensity fluctuations. This minimum persists albeit the clear presence of up-drafts (orange eddies, with positive vertical wind speed values) and down-drafts (blue eddies, with negative vertical wind speed values), and thus cannot be related to an aerosol layered structure in the mixing layer. Note that the backscatter minimum occurs preferably during up-drafts, but not during down-drafts. This behavior is clearly highlighted in figure 2, where the black dashed lines indicating the lidar backscatter minima only appear in temporal coincidence with the vigorous updrafts, which are testified by the positive vertical speed values (up to ~~5~~ 2-3 m s^{-1}) measured by the wind lidar, but do not appear in coincidence with the downdrafts (negative vertical speed values down to -~~5~~2-3 m s^{-1}). The presence of a persistent minimum in lidar backscatter at 1200 m, preferably during up-drafts, is also well visible in the particle backscattering coefficient~~range corrected backscatter lidar~~ data at 532 nm (not shown here). While we are concentrating on the time interval 12:00-13:00 UTC on 18 April 2013, additional evidence of this phenomenon was observed earlier and later in the day (i.e. 13:25-13:40, 13:50-14:05, 14:15-14:25, 14:35-15:00 UTC). The clear-air dark band phenomenon was also visible o~~i~~n other days (i.e. 20 April 2013) during HOPE, when the wind was blowing from directions overpassing the *Hambach* and *Inden* mines.

Figure 3 illustrates the vertical profile of β~~*RCS*~~$_{1064}$ ~~at~~ for the time interval 12:56:41-13:00:45 UTC on 18 April 2013 (~~1~~ 4 min average, green line), together with the vertical profiles of temperature, relative humidity (RH) and wind direction and speed, as measured by the radiosonde launched at 13:00 UTC from the near-by station of Hambach (4 km E-SE). ~~For the purpose of figure clarity, the *RCS*$_{1064}$ is only shown in the height interval 750-1500 m.~~ The clear-air dark band is found to extend from 1150 to 1275 m, with a vertical extension of 125 m and a minimum in ~~lidar~~ particle backscattering at 1225 m (backscatter reduction is ~~17~~8 %, corresponding to 0.~~4~~8 dB). This band takes place few hundred meters below both the Lifting

Condensation Level (LCL, at 1725 m or 814 mbar) and the freezing level (at 1630 m or 823.2 mbar). The figure reveals that wind is blowing from directions in the interval from 265° (at surface) to 232°. More specifically, the particle~~lidar~~ backscattering reduction is located in the same height region (1125-1450 m) where wind is found to blow from directions in the interval 232-240º, i.e. from the directions where the Tagebau Inden open-pit lignite mine is located. In general, CBL wind direction measurements by radiosondes may be difficult to interpret as they may reflect rotations taking place within the convective plumes. However, wind direction values (236-242°) similar to those measured by the radiosonde are also present in the same height interval in the 1 h (12:00-13:00 UTC) average wind direction profile measured by the wind lidar (figure 4), with values throughout the whole profile from 270° (at surface) to 230° (at 1600 m).

Figure 3 also reveals that the air at this height is characterized by RH values in the range 60-62 %. Lignite particles advected by the wind ~~on~~ to the lidar site are captured and ingested within the updrafts and downdrafts associated with the intensive convective activity present at the lidar site. As a result of the adiabatic cooling associated with the uplift, air-parcels undergo a sudden RH increase from values in the range 60-62 % (environmental RH values at the base of the dark band) to values in the range 75-80 % (these latter being the values reached within the lifting air-parcel assuming an ideal adiabatic cooling with no air entrainment into the convective plumes or external air ingestion within the lifting air-parcel). This sudden increase of RH has important effects on the size growth of the uplifted lignite aerosols.

Figure 5 illustrates the time–height cross-section of the particle depolarization ratio at 532 nm, δ_{532}, as measured by BASIL in the time interval 12:00-13:00 UTC on 18 April 2013, i.e. the same time interval considered in figure 2. Particle depolarization ratio, defined as the power ratio of the cross-polarized to the co-polarized components of the particle backscattering coefficient, provides an indication of the degree of asphericity of sounded particles. Particle depolarization depends not only on particles' shape, but also on their size and refractive index (among other, Burton *et al.*, 2015). Water-coated aerosols, wet haze, fog, cloud droplets, and small raindrops can be assumed to be almost spherical and are characterized by very small values of δ_{532}, typically not exceeding 0.03. Low depolarizing particles, usually smoke or urban aerosol, have depolarization ratios between 0.03 and 0.1 (e.g. Burton *et al.*, 2012), while high depolarizing particles, as desert or volcanic dust, have depolarization ratios varying between 0.25 and 0.35 (among others, Mona *et al.*, 2012).

~~Instead, particles with a more irregular shape are characterized by larger values of δ_{532}, typically exceeding 0.2.~~ A proper calibration of particle depolarization measurements requires accurate measurements of the cross- and co-polarized components of the particle backscattering coefficient. However, accurate measurements of these quantities may be difficult to obtain, often as a result of the depolarizing properties of different optical devices included in the receiver (Freudenthaler, 2016). This translates into a non-negligible uncertainty affecting particle depolarization measurements, which includes both a systematic component (bias) and a random component (statistical error). For the present lidar system, these two components were estimated to be 10 and 20 %, respectively (Di Girolamo *et al.*, 2012a).

Figure 5 reveals a decrease in particle depolarization at the same height and time intervals of the dark band. More specifically, δ_{532} decreases from values of 0.05-0.07 below the dark band to values of 0.02-0.03 within and above the dark

band. A decrease of δ_{532} within and above the dark band is compatible with the conjectured size growth of the uplifted dry lignite particles, initially having a more irregular shape, and then getting a more regular spherical shape as a result of the water uptake. Additionally, as previously observed for β_{1064}, the decrease of δ_{532} occurs during up-drafts, but not during down-drafts, as in fact during these latter values of δ_{532} are in the range 0.02-0.04 both below and within the dark band. However, both below and within the dark band, values of δ_{532} are rather low, which is typical of aerosols including a large portion of carbonaceous species as those resulting from fossil fuel combustion, having a rather spherical shape (Dieudonné *et al.*, 2017; Müller *et al.*, 2007). Particle depolarization ratio measurements, while providing some information on particle shape, may also be used for aerosol typing and mass concentration studies (among others, Petzold, 2011; Burton *et al.*, 2012).

The presence of the clear-air dark band phenomenon preferably during up-drafts is well documented also in figure ~~5~~6, illustrating the simultaneous vertical profiles of ~~βRCS_{1064}~~β_{1064} and RH as measured by BASIL, and the wind direction and vertical wind speed ~~(again~~as measured by the wind lidar~~)~~, for a number of consecutive up-drafts/down-drafts time intervals. Sharp lidar backscatter minima are only observed around 1200 m in temporal coincidence with positive vertical speed values (panels a, c, e, g), while slowly variable backscatter values are observed at these heights in temporal coincidence with negative vertical speed values (panels b, d, f, h). Speed direction values in the time intervals and vertical regions characterized by the presence of backscatter minima are very similar to those observed in these vertical regions during the downdraft periods. This observation supports the hypothesis that the observed backscatter minima are not caused by the presence and sounding of different types of particles which might originate from different aerosol sources, as in fact sounded air masses are coming from the same direction both during updrafts and downdrafts. However, it is to be specified that wind direction measurements by Doppler wind lidar require a minimum integration time of 5 minutes, as in fact a number of off-zenith measurements are needed to determine the horizontal wind component. This implies that a perfect time matching between BASIL measurements of β_{1064} and RH and wind lidar measurements of wind direction was not possible in figure 6, as in fact the integration time for BASIL measurements was taken coincident (within a of 10 sec, which is the maximum time resolution for BASIL measurements) with the duration of the updrafts and downdrafts, typically lasting 1-2 minutes, while the 5 min-integration time wind direction measurements may superimpose to consecutive updrafts/downdrafts. Additionally, the approach use to determine wind directions by Doppler wind lidar measurements is affected by a large uncertainty (typically around 25 degrees in the vertical regions characterized by the presence of backscatter minima).

Similar considerations apply for RH measurements. Accounting for the error bar affecting these measurements, RH values observed by BASIL in the altitude region where backscatter minima take place have very similar values sounded during the updraft and downdrafts, which would support the hypothesis of the presence of a reversal (evaporation) process in the downdrafts, which instead is not observed. It is to be pointed out that vertical profiles of RH are obtained from water vapour mixing ratio and temperature profile measurements by BASIL, which are based on the application of the vibrational and rotational Raman lidar technique, respectively. Both techniques rely on Raman backscatter phenomena characterized by

cross-sections which are several orders of magnitude smaller than the elastic backscatter cross-section. This makes the water vapour mixing ratio and temperature measurements, and consequently RH measurements, very difficult to perform, especially in daytime around noon, as is the case for the measurements illustrated in this paper, as a result of the large solar irradiance affecting the measurements during this portion of the day. This translates into a large statistical uncertainty affecting RH measurements, with a random error of 4-8 % (error bars in figure 6) in the altitude region (~ 1200 m) where the particle backscatter minima are observed.

Clear-air dark bands were mostly observed in the absence of a cloud topped CBL. However, few clouds were observed for this specific case study in the upper portion of the CBL at 12:53-13:00 UTC (orange-brown features in the upper panel of figure 2 and strong backscattering enhancement observed above 1600 m in figure 3). The occurrence of these clouds is discussed in more detail in the final portion of section 4.

~~Figure 6 illustrates the time-height cross section of the particle depolarization ratio at 532 nm, δ_{532}, as measured by BASIL in the time interval 12:00-13:00 UTC on 18 April 2013, i.e. the same time interval considered in figure 2. Particle depolarization ratio, defined as the power ratio of the cross-polarized to the co-polarized components of the particle backscattering coefficient, quantifies the degree of non-sphericity of sounded particles. Water-coated aerosols, wet haze, fog, cloud droplets, and small raindrops can be assumed to be almost spherical and are characterized by small values of δ_{532} typically smaller than 0.1. Instead, irregular-shape particles are characterized by values of δ_{532} typically exceeding 0.2. A proper calibration of particle depolarization measurements requires accurate measurements of the cross- and co-polarized components of the particle backscattering coefficient. However, accurate measurements of these quantities may be difficult to obtain, often as a result of the depolarizing properties of different optical devices included in the receiver (Freudenthaler, 2017). This translates into a non-negligible uncertainty affecting particle depolarization measurements, which includes both a systematic component (bias) and a random component (statistical error). For the present lidar system, these two components were estimated to be 10 and 20 %, respectively (Di Girolamo *et al.*, 2012a).~~

~~Figure 7 reveals a decrease in particle depolarization at the same height and time intervals of the dark band. More specifically, δ_{532} range from values of 0.30-0.35 below the dark band to values of 0.15-0.20 within and above the dark band. A decrease of δ_{532} within and above the dark band is compatible with the size growth of the uplifted dry lignite particles, initially having a more irregular shape, and then getting a more regular spherical shape as a result of the water uptake. Additionally, as previously observed for RCS_{1064}, the decrease of δ_{532} occurs during up-drafts, but not during down-drafts.~~

4 Hygroscopic and scattering behavior of lignite particles

Aerosol particles can be classified according to their affinity for water as hygroscopic, neutral or hydrophobic. The characterization of particle hygroscopicity is of primary importance in climate monitoring and prediction. Model studies have demonstrated that RH has a critical influence on aerosol climate forcing (Pilinis *et al.*, 1995), with hygroscopic growth at large RH values having important implications in terms of aerosol direct effect (Wulfmeyer and Feingold, 2000).

Lignite, often referred to as brown coal, is a combustible sedimentary rock formed from naturally compressed peat, with a carbon content around 60-70 %. The high moisture content of lignite (approximately 50 - 60%) is an undesirable inert component, which significantly reduces its calorific value. Consequently, when employed in conventional power plants, a considerable portion of lignite's energy content is typically required prior to combustion to evaporate this high portion of water. For this reason, following the mining process, raw lignite usually undergoes effective drying processes. This is indeed the case for the two open-pit lignite mines of *Tagebau-Hambach* and *Tagebau Inden* in the proximity of the lidar station, where a drying process based on the pulverization of the lignite particles is applied.

Dried lignite particles produced in open pit lignite mines have a very marked hygroscopic behavior (Schobert, 1995; Krawczykowska, and Marciniak-Kowalska, 2012) and, as a result of this behavior, effectively absorb moisture from the atmosphere. Measurements of the particle size distribution of lignite particles escaped from heavy industrialized areas (mining and power stations operations) in the form of fly ash or fugitive dust have been reported by several authors (among others, Triantafyllou *et al*., 2006; Civiš, M., and Jan Hovorka, J., 2010). Specifically, Triantafyllou *et al*. (2006) were able to measure the particle size distribution of fly ash injected into the atmosphere from elevated stacks in power stations, identifying a prominent particle mode at ~ 8 μm, with approximately 80% of the particles smaller than 10 μm. Civiš and Hovorka (2010) reported size distribution measurements for brown coal with an average particle size of 1.84 μm. All these authors revealed a limited degree of poly-dispersion of atmospheric lignite particles. When considering a log-normal size distribution, the degree of poly-dispersion or width of the particle size distribution is expressed in terms of the percentage standard deviation of the logarithm of the distribution, σ. Narrow size distributions for brown coal particles, with values of σ in the interval 5-10 %, have been reported by a variety of authors (Mujuru *et al*., 2009; Civiš and Hovorka, 2010, Wang and Tichenor, 1981)**.**

The solution effect typically dominates hygroscopic particles' growth when the radius is small (smaller than the critical radius r_c), which results in small solution droplets being in equilibrium with water vapour at RH values less than 100 % (Yau and Rogers, 1989). At this stage, small increases in RH determine particles' size growth until equilibrium is newly reached. This mechanism is possibly responsible for the lignite particle growth below the LCL, ultimately leading to the appearance of a minimum in lidar backscatter echoes (i.e. the above mentioned clear-air dark band phenomenon). The increase in particles' radius associated with the relative humidity change experienced by the adiabatically uplifted air-parcel can be estimated based on the application of the Köhler equation. When RH values are smaller than 100 %, the Köhler equation is dominated by the solution term, which depends on the mass and molecular weight of the solute species and the so called van't Hoff factor. Based on literature values of these quantities, t~~T~~he above specified ~~change~~ increase of RH from 60-62 to 75-80 % would ~~accordingly~~ result in a particle size growth in radius by ~~--~~10~~5~~ ~~30~~ 20 %. In this study, we are considering an initial size for the dry lignite particles of 1.84 and 8 μm, as reported by Civiš and Hovorka (2010) and Triantafyllou *et al*. (2006), respectively.

Scattering properties of lignite particles have been simulated based on the application of a light scattering code for spheres based on Mie theory (http://philiplaven.com/mieplot.htm). In this respect it is to be specified that the small values of δ_{532}

characterizing the observed aerosol particles call for a very limited degree of asphericity, which makes Mie theory still successfully applicable for the simulation of particles' scattering properties (Martin, 1993; Mishchenko and Lacis, 2003). In order to properly simulate the scattering processes, accurate information on particle refractive index are required, besides those on particle size distribution already provided above. Accurate measurements of lignite refractive index were reported by Lohi *et al*. (1992), who observed values of the real and imaginary part of the complex refractive index of 1.70 and $1x10^{-6}$, respectively. Similar values have were reported by McCartney and Ergun (1962) and Read (2008). Simulations of the scattering properties of lignite particles are illustrated in figure 7. The figure shows the variability of the quantity $Q_{back} \times r^2$ ~~backscattering efficiency, Q_{back},~~ as a function of r ~~particle radius~~, with Q_{back}, being the backscattering efficiency and r being the particle radius. These simulations are obtained by considering a log-normal size distribution with a value of σ of 5 %. The simulation in the upper panel of the figure considers a minimum radius of 1.84 μm, as measured by Civiš and Hovorka (2010), while the simulation in the lower panel considers a minimum radius of 8 μm, as measured by Triantafyllou *et al*. (2006). Both simulations consider a sounding wavelength of 1.064 μm, which is the laser wavelength used for the dark band lidar measurements illustrated in figure 2. The quantity $Q_{back} \times r^2$ represents the single-particle backscattering coefficient, assuming a constant particle number density n. Figure 7 reveals the presence of marked oscillations in particle backscattering efficiency. As a result of these oscillations, for specific radius values of the dry lignite particles (for example, ~~2.4~~6.5 μm, ~~7~~3.5~~8~~ μm, ~~16.5~~18 μm, ~~28~~ 28.5 μm, 4~~10~~ μm), a reduction in $Q_{back} \times r^2$ ~~backscatter efficiency~~ of 8-27 % (~~approximately~~ 0.35-1.4 dB) is observed for a particle size growth by 1~~05~~ ~~30~~ 16 %, which is compatible with the size growth experienced by these particles during their adiabatic ascent. Thus, we believe that the observed dark band phenomenon is associated with the oscillations in the particle backscattering coefficient~~efficiency~~, ultimately leading to Mie back-scattered signal intensity fluctuations. These backscattering coefficient~~efficiency~~ oscillations are to be attributed to the limited degree of poly-dispersion of atmospheric lignite particles. It is to be specified that these oscillations smooth down and finally disappear in case larger values of σ, i.e. wider particle size distributions (distributions with a higher degree of poly-dispersion), are considered. This is clearly highlighted in figure 8, which illustrates the simulated values of Q_{back} for lignite particles as a function of particle radius, considering a log-normal size distribution with different values of σ (0.1, 5, 10 and 20 %), again considering a sounding wavelength of 1.064 μm. As for figure 7, the simulation in the upper panel considers a minimum radius of 1.84 μm, as measured by Civiš and Hovorka (2010), while the simulation in the lower panel considers a minimum radius of 8 μm, as measured by Triantafyllou *et al*. (2006). The figure clearly reveals that both in the smaller and larger particles domain, the consideration of progressively larger values of σ leads to a progressive smearing down of the Q_{back} oscillations, which are still present for values of $\sigma \leq 10$ %, but are almost absent for $\sigma = 20$ %.

An additional quantity, namely the backscatter color ratio, *BCR*, i.e. the ratio of total backscattering coefficients at 1064 and 532 nm, was determined from BASIL measurements. Color ratio profiles measured during the time interval considered in the present study (12:00-13:00 UTC on 18 April 2013, not shown here) indicate values in the range 0.40-0.45 below the dark band and in the range 0.33-0.36 within the dark band region. The color ratio decrease is an indication of the increase of

particle size. This represents an additional experimental evidence of the conjectured particles' growth, which represents the basis of the given interpretation of the observed phenomenon. Furthermore, small backscatter color ratio values, as those found both below and within the dark band, are indicating relatively large particles (Burton *et al.*, 2013), compatible with those conjectured in the present study and presently considered in our simulations. The variability of backscatter color ratio as a function of particle radius has been simulated with the same Mie scattering code already used above, with simulations revealing that values of *BCR* in the range 0.33-0.45 are compatible with particle size in the range 7-11 μm. Finally, backscatter color ratio values in the range 0.33-0.45 combined with values of δ_{532} in the range 0.02-0.07 are in agreement with previously observed values of these quantities as reported by a variety of authors (de Villiers *et al.*, 2010, *BCR*=0.3-0.5 and δ_{532}=0.02-0.08; Burton *et al.*; 2014, *BCR*=0.55 and δ_{532}=0.07; Burton *et al.*, 2015, *BCR*=0.47 and δ_{532}=0.06-0.09). Similar values (*BCR*=0.35-0.54 and δ_{532}<0.05) were also reported by Franke *et al.* (2003) and Müller *et al.* (2007) for Southeast Asian aerosols, which were argued to possess a pronounced coarse mode, with large particles being originated mainly from coal and dried plants used for domestic heating and cooking (Müller *et al.*, 2007).

The comparison of simulated values of single-particle backscattering coefficient $Q_{back} \times r^2$ (~ 3×10^{-11} m^2 sr^{-1} for a particle radius of 4 μm and ~ 1×10^{-9} m^2 sr^{-1} for a particle radius of 20 μm) with measured values of the volume backscattering coefficient β_{1064} (in figures 5, in the range 2.5-3.5$\times 10^{-6}$ m^{-1} sr^{-1} within the dark band) leads to an estimate of particle number density *n* of 0.8-1.2$\times 10^5$ m^{-3} and 2.5-3.5$\times 10^3$ m^{-3} in the small and large particles' domain, respectively. These values of *n* are in agreement with literature values for continental and urban polluted aerosols (among others, Mészáros, 1991, 0.8-3.5$\times 10^5$ m^{-3} for a particle radius of 4 μm and 1-2$\times 10^3$ m^{-3} for a particle radius of 20 μm).

The solution effect growth of particles to equilibrium size associated with increasing RH can be continued up to a RH value of 100 % and slightly beyond. Cloud formation at the top of the CBL will finally take place above the LCL if the critical saturation ratio, S_c, corresponding to the peak of the Koehler curve, is reached. S_c is typically reached for super-saturation values of 0.5-1%, depending on the composition (and consequently the level of hygroscopicity) and size of the aerosol particle acting as condensation nuclei. In the case of lignite particles, typical values of S_c and of the critical radius, r_c, are in the range 0.5-1% and 1-10 μm, respectively. Up to this point RH had to be increased in order for the droplet to grow. However, if RH slightly exceeds S_c, the particle is enabled to grow beyond r_c and its saturation ratio falls below S_c. As a consequence, the water vapour condensates on the droplet, which will continue to grow without the need for a further increase in saturation ratio (Yau and Rogers, 1989). When this occurs, clouds can form on the top of the CBL. These processes are responsible for the clouds observed in the upper portion of the CBL at 12:53-13:00 UTC (orange-brown features in the upper panel of figure 2). In the clouds, the droplet growth process does not continue indefinitely as many droplets are present and all of them compete for the same available water vapour.

5 Discussion of the observed phenomena

Raman lidar measurements illustrated in this paper reveal the presence of a persistent minimum (dark band) in lidar elastic backscatter echoes in the upper portion of the CBL. This phenomenon appears in clear sky conditions in the presence of strong convective activity and is mostly confined to updrafts. Adiabatic cooling within the updrafts leads to an RH increase and a consequent particles' growth, especially of hygroscopic particles. If we assume that most of the particles we observe are dry hygroscopic lignite particles from the surrounding lignite open-pit mines and their size distribution is mono-disperse or very narrow, we must conclude that the observed dark band is related to the oscillations of the backscatter efficiency as described by Mie-theory, ultimately leading to intensity fluctuations of the Mie back-scattered radiation. In the presence of a wider particle size distribution the backscatter oscillations should smear out, if not disappear. This interpretation is also supported by the outcome of the lidar depolarization measurements. In fact, water uptake by uplifted dry lignite aerosols, initially having a more irregular shape, confers a more regular spherical shape to these particles, this shape change being responsible for the decrease in particle depolarization observed at the same height and time intervals of the dark band (figure 6), again mostly confined to updrafts.

The fact that the dark band and the depolarization decrease are confined to the up-drafts can be explained in two ways: either the adiabatic warming, and the consequent decrease in RH, in down-drafts does not lead to an inversion of the particle growth, i.e. there is a hysteresis, and humidified particles do not evaporate the water amount they incorporated during their way up. Or down-drafts transport other or modified particles than the up-drafts. These particles might be less hygroscopic and thus change their size less with RH. The possibility that particles within the down-drafts are different from those within the up-drafts increases in the interfacial layer due to the entrainment effects and is ~~also~~ possibly testified by the presence of smaller particle backscatter values ~~observed~~ within the down-drafts with respect to those observed within the up-drafts (see figure 2). This is possibly associated with the entrainment of air from the free-troposphere at the top of the CBL, which may ultimately lead to changes in particle size distribution and scattering properties. Evidence of the sharp entrainment of air pockets from the free troposphere into the boundary layer, which gradually mix with the environmental air, has been reported by a variety of authors (Couvreux et al., 2005, 2007; Wulfmeyer et al., 2010, 2016; Turner et al., 2014). Particle size distribution within the down-draft could be not as narrow as in the updrafts, resulting in a smear out of backscatter efficiency oscillations.

Few more words should be spent on these aspects. The hygroscopic growth of particles is dependent upon aerosol composition and may be monotonic (smoothly varying) or deliquescent (step change) growth. A dry hygroscopic aerosol transforms into a solution droplet when RH increases beyond the so called deliquescence point. Particle deliquescent growth, as the one characterizing lignite particles (Brooks *et al.*, 2004), shows an hysteresis behavior during the uptake and loss of water, i.e. exhibit difference values for the deliquescence and efflorescence relative humidity (Sjogren *et al.*, 2007); this hysteresis behavior ultimately determines a less efficient evaporation process (Seinfeld and Pandis, 2006). More specifically, when RH decreases, the solution droplet starts reducing in size through the evaporation of the previously up-taken water at the efflorescence point, which is found at a much lower RH value than the deliquescence point (Oatis *et al.*, 1998).

6 Summary and final remarks

This paper illustrates measurements carried out by the Raman lidar system BASIL in the frame of HOPE, revealing the presence of a persistent minimum in clear-air backscatter echoes in the upper portion of the convective boundary layer. Backscatter reduction is approximately 10 % ~~dB~~, has a vertical extent of approximately 100 m and persists over a period of several hours. We refer to this phenomenon as to the *clear-air dark band* or the *convective dark band*. This has to be distinguished from a similar phenomenon, with comparable temporal duration and backscatter reduction, observed in the presence of light precipitation events (Sassen and Chen, 1995; Demoz *et al*., 2000), the so called *lidar dark band*, ascribable to the changes in precipitating particles' scattering properties taking place during the snowflake-to-raindrop transition.

Dark bands illustrated in this paper are observed in the presence of strong convective activity within the boundary layer, when dry lignite aerosol particles are advected from the surrounding open pit mines; the bands are mostly confined to the convective updrafts. The phenomenon is interpreted as being related to the oscillations characterizing lignite particle backscatter efficiency, ultimately leading to Mie back-scattered signal intensity fluctuations. These backscatter efficiency oscillations are attributed to the limited degree of poly-dispersion and the high hygroscopicity of atmospheric lignite particles. Adiabatic cooling within the updrafts leads to an RH increase and a consequent particles' growth.

Adiabatically warming and thus decrease in RH in down-drafts does not lead to an inversion of the particle growth and humidified particles do not or only partially evaporate the water they took up during their way up. Additionally, down-drafts may transport other particles than the up-drafts. These are possible motivations for having clear-air dark bands mostly confined to updrafts. Observations and results illustrated in this paper support the interpretation of the phenomenon as a purely microphysical growth mechanism; however, the possibility that other mechanisms (for example, dynamics) may also participate and contribute to the appearance of the phenomenon cannot be completely excluded.

References

Bhawar, R., P. Di Girolamo, D. Summa, C. Flamant, D. Althausen, A. Behrendt, C. Kiemle, P. Bosser, M. Cacciani, C. Champollion, T. Di Iorio, R. Engelmann, C. Herold, D. Müller, S. Pal, M. Wirth and V. Wulfmeyer: The water vapour intercomparison effort in the framework of the Convective and Orographically-induced Precipitation Study: airborne-to-ground-based and airborne-to-airborne Lidar systems, Q. J. Roy. Meteor. Soc., 137, 325-348, doi: 10.1002/qj.697, 2011.

Brooks, S. D., P. J. DeMott, S. M. Kreidenweis: Water uptake byparticles containing humic materials and mixtures of humic materials with ammonium sulfate, Atm. Envir., 38, 1859–1868, 2004.

Burton, S. P., Ferrare, R. A., Hostetler, C. A., Hair, J.W., Rogers, R. R., Obland, M. D., Butler, C. F., Cook, A. L., Harper, D. B., and Froyd, K. D.: Aerosol classification using airborne High Spectral Resolution Lidar measurements – methodology and examples, Atmos. Meas. Tech., 5, 73–98, doi:10.5194/amt-5-73-2012, 2012.

Burton, S. P., Ferrare, R. A., Vaughan, M. A., Omar, A. H., Rogers, R. R., Hostetler, C. A., and Hair, J. W.: Aerosol classification from airborne HSRL and comparisons with the CALIPSO vertical feature mask, Atmos. Meas. Tech., 6, 1397–

1412, doi:10.5194/amt-6-1397-2013, 2013.

Burton, S. P., Vaughan, M. A., Ferrare, R. A., and Hostetler, C. A.: Separating mixtures of aerosol types in airborne High Spectral Resolution Lidar data, Atmos. Meas. Tech., 7, 419–436, doi:10.5194/amt-7-419-2014, 2014.

Burton, S. P., Hair, J. W., Kahnert, M., Ferrare, R. A., Hostetler, C. A., Cook, A. L., Harper, D. B., Berkoff, T. A., Seaman, S. T., Collins, J. E., Fenn, M. A., and Rogers, R. R.: Observations of the spectral dependence of linear particle depolarization ratio of aerosols using NASA Langley airborne High Spectral Resolution Lidar, Atmos. Chem. Phys., 15, 13453-13473, https://doi.org/10.5194/acp-15-13453-2015, 2015.

Civiš, M., and ~~Jan~~ Hovorka, J.: Characterization of main dust samples from a surface lignite mine using a resuspension chamber, J. Res. Applic. Pr*o*f. Security, 3, 3-4, 2010.

Couvreux, F., Guichard, F., Redelsperger, J.-L., Kiemle, C., Masson, V., Lafore, J.-P., and Flamant, C.: Water-vapour velocity within a convective boundary layer assessed by large-eddy simulations and IHOP_2002 observations. Q. J. Roy. Meteor. Soc., 131, 2665–2693, doi:10.1256/qj.04.167, 2005.

Demoz, B. B., Starr, D., Whiteman, D., Evans, K., Hlavka, D., and Peravali, R.: Raman LIDAR Detection of Cloud Base, Geophys. Res. Lett., 27, 1899–1902, 2000.

Di Girolamo, P., Demoz, B. B., and Whiteman, D. N: Model simulations of melting hydrometeors: A new lidar bright band from melting frozen drops, Geophys. Res. Lett., 30, 1626, doi:10.1029/2002GL016825, 2003.

Di Girolamo P., R. Marchese, D. N. Whiteman, and B. B. Demoz.: Rotational Raman Lidar measurements of atmospheric temperature in the UV, Geophys. Res. Lett., 31, L01106, doi: 10.1029/2003GL018342, 2004.

Di Girolamo, P., A. Behrendt, and V. Wulfmeyer: Spaceborne profiling of atmospheric temperature and particle extinction with pure rotational Raman Lidar and of relative humidity in combination with differential absorption Lidar: performance simulations, Appl. Opt., 45, 2474-2494, doi: 10.1364/AO.45.002474, 2006.

Di Girolamo, P., Summa, D., and Ferretti, R.: Multiparameter Raman Lidar Measurements for the Characterization of a Dry Stratospheric Intrusion Event, J. Atmos. Ocean. Technol., 26, 1742–1762, doi:10.1175/2009JTECHA1253.1, 2009a.

Di Girolamo, P., Summa, D., Lin R.-F, Maestri T, Rizzi R, G. Masiello: UV Raman Lidar measurements of relative humidity for the characterization of cirrus cloud microphysical properties. Atmos. Chem. Phys., 9, 8799-8811, doi: 10.5194/acp-9-8799-2009, 2009b.

Di Girolamo, P., D. Summa, R. Bhawar, T. Di Iorio, M. Cacciani, I. Veselovskii, O. Dubovik, A. Kolgotin: Raman Lidar observations of a Saharan dust outbreak event: Characterization of the dust optical properties and determination of particle size and microphysical parameters. Atm. Env., 50, 66-78, ISSN: 1352-2310, doi: 10.1016/j.atmosenv.2011.12.061, 2012a.

Di Girolamo, P., Summa, D., Cacciani, M., Norton, E. G., Peters, G., and Dufournet, Y.: Lidar and radar measurements of the melting layer: observations of dark and bright band phenomena, Atmos. Chem. Phys., 12, 4143–4157, doi:10.5194/acp-12-4143-2012, 2012b.

Di Girolamo, P., Flamant, C., Cacciani, M., Richard, E., Ducrocq, V., Summa, D., Stelitano, D., Fourrié, N., and Saïd, F.: Observation of low-level wind reversals in the Gulf of Lion area and their impact on the water vapour variability, Q. J. Roy. Meteor. Soc., 142, 153–172, doi:10.1002/qj.2767, 2016.

Di Girolamo, P., D. Summa, B. De Rosa, M. Cacciani, A. Scoccione, A. Behrendt, V. Wulfmeyer: Characterization of Boundary Layer Turbulent Processes by Raman Lidar: Demonstration of the Measurement Capabilities of the Raman Lidar System BASIL, Atmos. Chem. Phys., 17, 745-767, doi:10.5194/acp-17-745-2017, 2017.

Dieudonné, E., Chazette, P., Marnas; F., Totems, J., Shang, X.: Raman Lidar Observations of Aerosol Optical Properties in 11 Cities from France to Siberia, Remote Sens. 2017, 9, 978; doi:10.3390/rs9100978, 2017.

Freudenthaler, V.: ~~Polarisation effects in lidar signals: determination, correction, and uncertainty calculation, Proceedings of the 28th International Laser Radar Conference, paper 201, Bucharest (Romania), 25-30 June 2017.~~About the effects of polarising optics on lidar signals and the Δ90 calibration, Atmos. Meas. Tech., 9(9), 4181–4255, doi:10.5194/amt-9-4181-2016, 2016.

Franke, K., A. Ansmann, D. Mu¨ller, D. Althausen, C. Venkataraman, M. S. Reddy, F. Wagner, and R. Scheele, Optical properties of the Indo-Asian haze layer over the tropical Indian Ocean, J. Geophys. Res., 108(D2), 4059, doi:10.1029/2002JD002473, 2003.

Griaznov, V., I. Veselovskii, P. Di Girolamo, M. Korenskii, D. Summa: Spatial Distribution of Doubly Scattered Polarized Laser Radiation in the Focal Plane of a Lidar Receiver, Appl. Opt, 46, 6821-6830, doi: 10.1364/AO.46.006821, 2007.

Groß, S., Freudenthaler, V., Schepanski, K., Toledano, C., Schäfler, A., Ansmann, A., and Weinzierl, B.: Optical properties of long-range transported Saharan dust over Barbados as measured by dual-wavelength depolarization Raman lidar measurements, Atmos. Chem. Phys., 15, 11067-11080, https://doi.org/10.5194/acp-15-11067-2015, 2015.

Krawczykowska, A., and Marciniak-Kowalska, J.: AGH Journal of Mining and Geo-engineering, 36 (4), 57-65, 2012.

Lohi, A., Wynnyckyj, J. R., Rhodes, E.: Spectral measurement of the complex refractive index of fly ashes of canadian lignite and sub-bituminous coals, Can. J. Chem. Eng., 70, 751-758, 1992.

Macke, A., P. Seifert, H. Baars, C. Beekmans, A. Behrendt, B. Bohn, B. Lakshmi Madhavan, E. Hammann, R. Heinze, J. Bühl, S. Crewell, T. Damian, P. Di Girolamo, J. Kalisch, N. Kalthoff, S. Kinne, U. Löhnert, S. Muppa, I. Serikov, H. Siebert, C. Simmer, F. Späth, S. Steinke, K. Träumner, B. Wehner, A. Wieser, X. Xie: The HD(CP)2 Observational Prototype Experiment HOPE - An Overview, Atmos. Chem. Phys., 17, 4887–4914, doi:10.5194/acp-17-4887-2017, 2017.

McCartney, J. T., and Ergun, S.: Refractive Index and Thickness of Ultrathin Sections of Coals and Graphite by Interferometry, Journal of the Optical Society of America, 52 (2), 197-200, 1962.

Martin, R. J.: Mie Scattering Formulae for Non-spherical Particles, Journal of Modern Optics Vol. 40, Iss. 12, 1993.

Mészáros, E.: The atmospheric aerosol, in Atmospheric particles and Nuclei, G, Götz, E. Mészáros, and G. Vali, Eds., Akadémiai Kiado, Budapest, 17-84, 1991.

Mishchenko, M. I. and A. A. Lacis,: Morphology-dependent resonances of nearly spherical particles in random orientation," Appl. Opt. 42, 5551-5556, 2003.

Mona, L., Liu, Z., Müller, D., Omar, A., Papayannis, A., Pappalardo, G., Sugimoto, N., and Vaughan, M.: Lidar Measurements for Desert Dust Characterization: An Overview, Advances in Meteorology, 2012, 356265, doi:10.1155/2012/356265, 2012.

Müller, D., A. Ansmann, I. Mattis, M. Tesche, U. Wandinger, D. Althausen, and G. Pisani: Aerosol-type-dependent lidar ratios observed with Raman lidar, J. Geophys. Res., 112, D16202, doi:10.1029/2006JD008292, 2007.

Mujuru, M., R. I. McCrindle, and N. Panichev, Characterisation of coal slurries for introduction into ICP OES for multi-element determinations, J. Anal. At. Spectrom., 24, 494-501, 2009.

Oatis, S., D. Imre, R. McGraw, and J. Xu, Heterogeneous nucleation of a common atmospheric aerosol: Ammonium sulfate, Geophys. Res. Lett., 25 (24), 4469-4472, 1998.

Petzold, A.: STSE—ICAROHS—inter-comparison of aerosol retrievals and observational requirements for multi-wavelength HSRL systems, Final Report. Tech. rep., ESA, 2011.

Pilinis, C., Pandis, S.N., Seinfeld, J.H.: Sensitivity of a direct climate forcing by atmospheric aerosols to aerosol size and composition, J. Geophys. Res., 100, 18739-18754, 1995.

Read P.G.: Gemmology, 3rd ed. Elsevier Butterworth-Heinemann, Oxford, UK, 2008.

~~Yau, M.K., R R Rogers: A Short Course in Cloud Physics 3rd Edition, **ISBN:** 9780750632157, **eBook ISBN:** 9780080570945, Ed. Butterworth Heinemann, pp. 304, 1989.~~

Sassen, K. and Chen, T.: The lidar dark band: An oddity of the radar bright band, Geophys. Res. Lett., 22, 3505-3508, 1995.

Sassen, K., Campbell, J. R., Zhu, J., Kollias, P., Shupe, M., and Williams, C.: Lidar and triple-wavelength Doppler radar measurements of the melting layer: A revised model for dark and bright band phenomena, J. Appl. Meteor. , 44, 301–312, 2005.

Schobert, H.H.: Lignites of North America, Series: Coal Science and Technology, Volume 23, pp. 695, Elsevier Science, eBook ISBN: 9780080544625, 1995.

Seinfeld, J. H. and Pandis, S. N.: Atmospheric Chemistry and Physics: From Air Pollution to Climate Change, 2nd, Wiley, New York, 2006.

Sjogren, S., M. Gysel, E.Weingartner, U. Baltensperger, M.J. Cubison, H. Coe, A.A. Zardini, C. Marcolli, U.K. Krieger, T. Peter, Hygroscopic growth and water uptake kinetics of two-phase aerosol particles consisting of ammonium sulfate, adipic and humic acid mixtures, Aerosol Science, 38, 157-171, 2007.

Triantafyllou, A. G., Zoras, S., Evagelopoulos V.: Particulate matter over a seven year period in urban and rural areas within, proximal and far from mining and power station operations in Greece, Environ. Monitor. and Assess., 122, 41-60, 2006.

Wang, J. C. F., and D. A. Tichenor, Particle size measurements using an optical variable-frequency-grid technique, Appl. Opt., 20, 1367-1373, 1981.

Turner, D. D., Wulfmeyer, V., Berg, L. K., and Schween, J. H.: Water vapor turbulence profiles in stationary continental convective mixed layers, J. Geophys. Res. 119, 11151–11165, DOI:10.1002/2014JD022202, 2014.

Wulfmeyer, V., Feingold, G.: On the relationship between relative humidity and particle backscattering coefficient in the marine boundary layer determined with differential absorption lidar, J. Geophys. Res., 105, 4729-4741, 2000.

Wulfmeyer, V., Turner, D. D., Pal, S., and Wagner, E.: Can water vapour Raman lidar resolve profiles of turbulent variables in the convective boundary layer?, Bound.-Lay. Meteorol., 136, 253–284, doi:10.1007/s10546-010-9494-z, 2010.

Yau, M. K., and R R Rogers: A Short Course in Cloud Physics - 3rd Edition, ISBN: 9780750632157, eBook ISBN: 9780080570945, Ed. Butterworth-Heinemann, pp. 304, 1989.

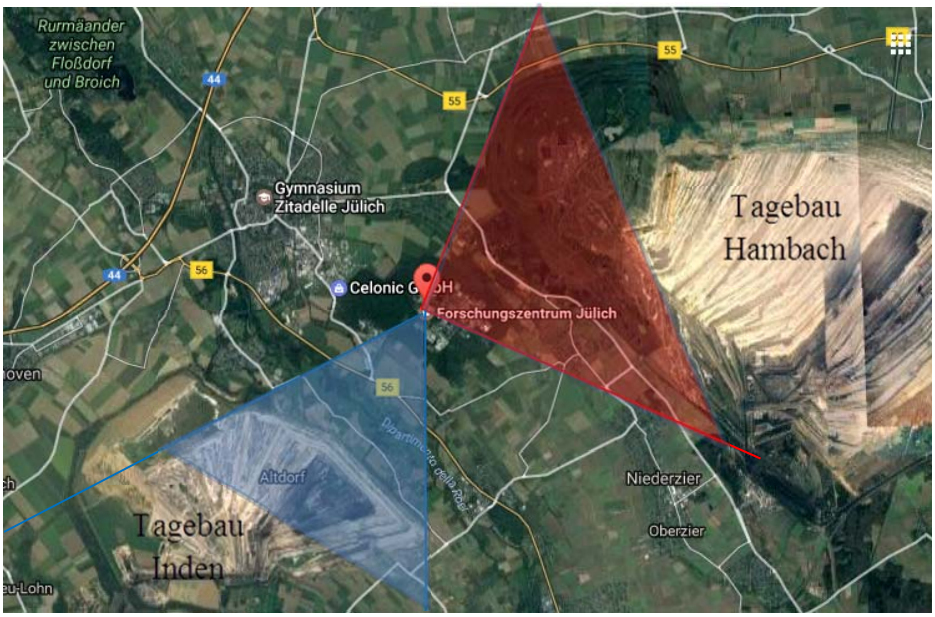

Figure 1: Locations of the Raman lidar system BASIL within the Jülich Research Centre (pink dot). The figure also indicates the location of the Tagebau-Hambach open-pit lignite mine (approximately 3 km East of the Research Centre), the large artificial hill Sophienhöhe (both within the angle cone 29-114°, red shaded area) and a second open-pit lignite mine (approximately 3 km South-West of the Research Centre, within the angle cone 180-240° blue shaded area).

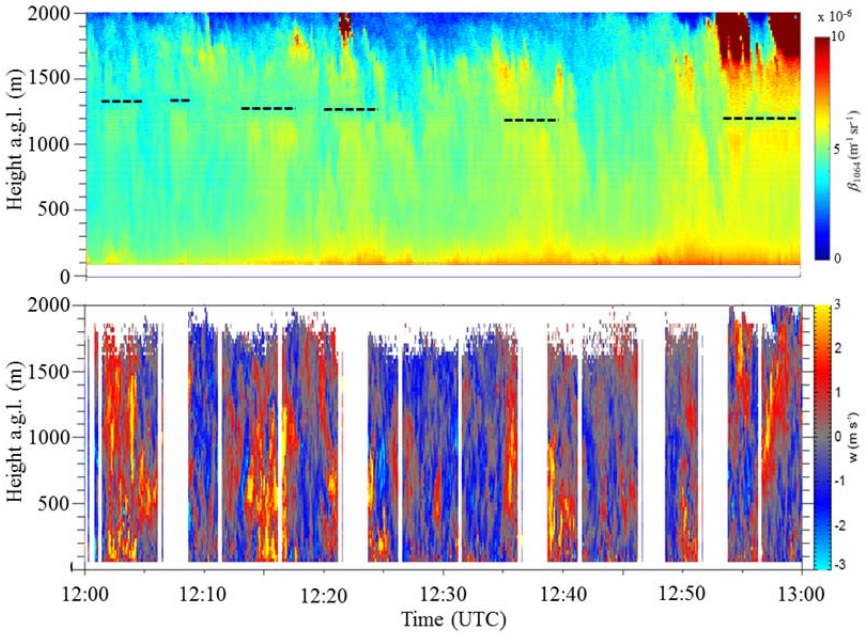

Figure 2: Time–height cross-section of ~~βRCS_{1064}~~$_{1064}$ (upper panel) and the vertical wind speed (lower panel) in the time interval 12:00 - 13:00 UTC on 18 April 2013~~. ~~RCS_{1064} is expressed in arbitrary units with low to mid to high values represented with blue to green to red.~~ The black dashed line in the upper panel around 1200 m highlights the presence of a persistent lidar backscatter reduction (clear-air dark band), with alternating intensity fluctuations.

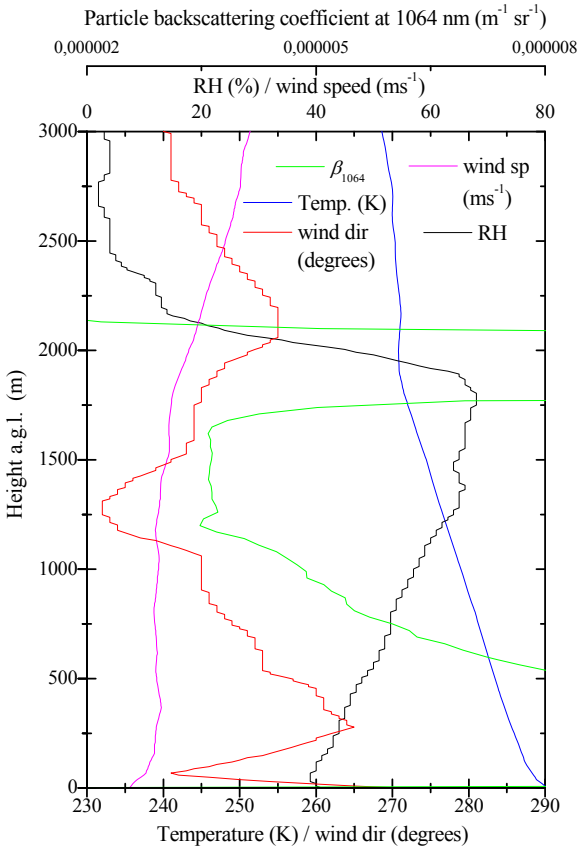

Figure 3: Vertical profile of β_{1064} at 13:00 UTC on 18 April 2013 (~~1 min average~~12:56:41-13:00:45 UTC, green line), together with the vertical profiles of temperature (blue line), RH (black line) and wind direction (red line) and speed (purple line) as measured by the radiosonde launched at 13:00 UTC from the near-by station of Hambach (4 km E-SE).~~ For the purpose of clarity of the figure the green line is only shown in the height interval 750-1500 m.

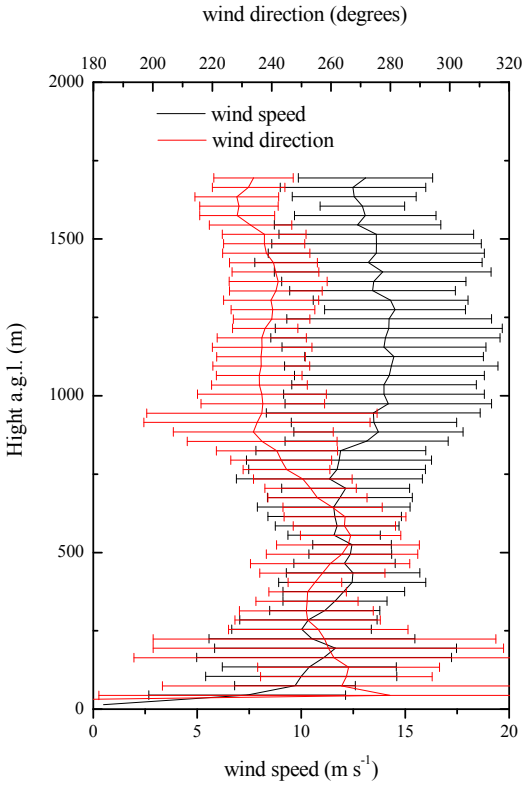

Figure 4: Vertical profile of wind speed and direction averaged over the time interval 12:00-13:00 UTC on 18 April 2013 as measured by the wind lidar located in the proximity of BASIL at the Supersite JOYCE. Profiles are reported with error bars, corresponding to ± 1 standard deviation.

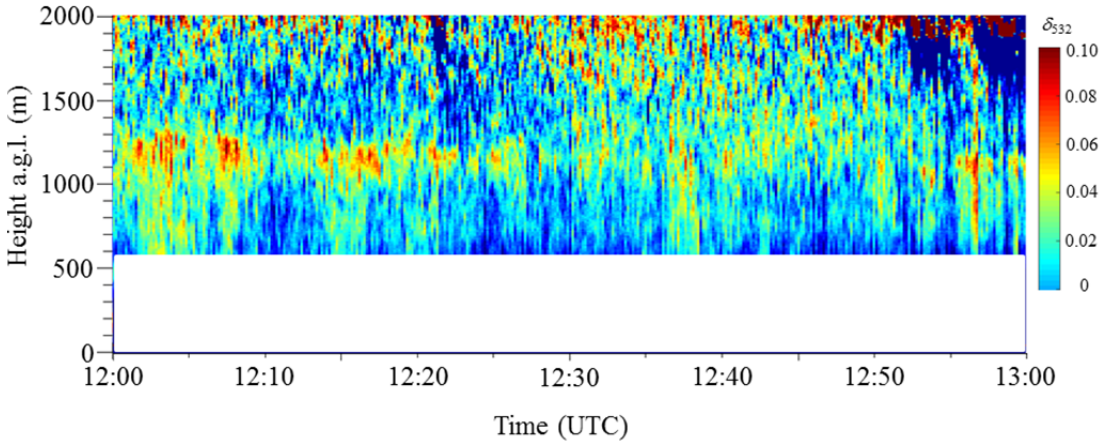

Figure 5: Time–height cross-section of particle depolarization at 532 nm in the time interval 12:00 - 13:00 UTC on 18 April 2013.

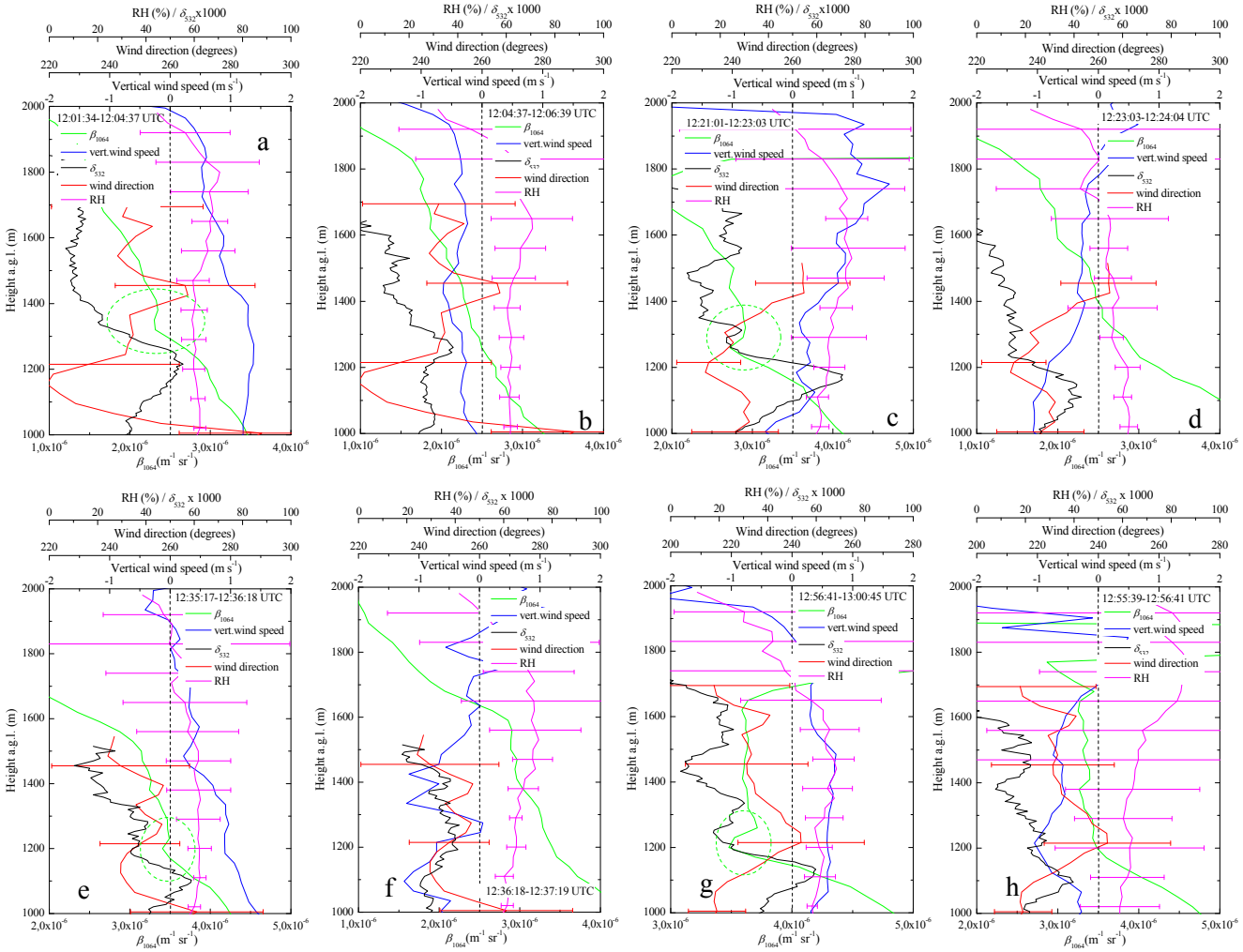

Figure ~~5~~6: Vertical profiles of *~~βRCS~~$_{1064}$* and RH (as measured by BASIL) and the wind direction and vertical wind speed ~~(again~~as measured by the wind lidar) ~~the vertical wind speed (again measured by the wind lidar)~~ for eight consecutive up-drafts/down-drafts time intervals during the time period 12:00-13:00 UTC on 18 April 2013: a) 12:01:34-12:04:37, b) 12:04:37-12:06:39, c) 12:21:01-12:23:03 UTC, d) 12:23:03-12:24:04 UTC, e) 12:35:17-12:36:~~19~~18 UTC, f) 12:36:18-12:37:19 UTC, g) 12:56:41-13:00:45 UTC, h) 12:55:39-12:56:41 UTC). Green-dashed ellipses highlight dark band features during the updraft intervals.

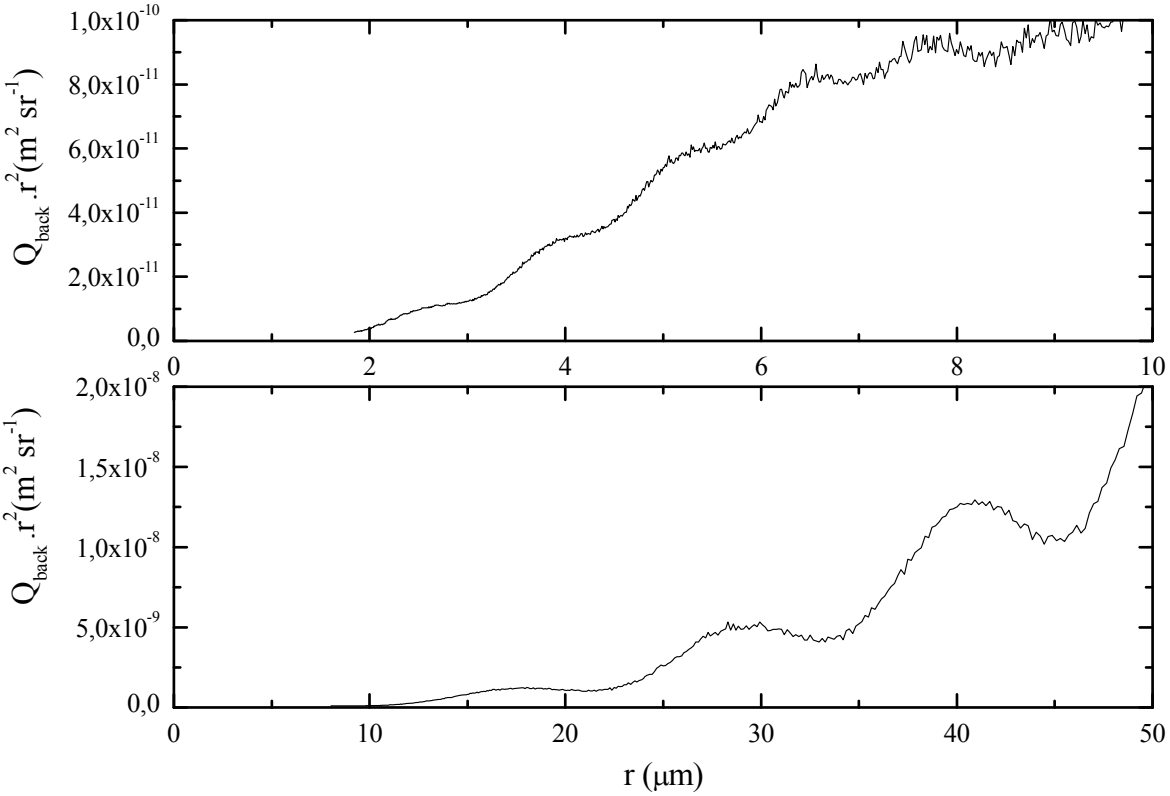

Figure 7: Simulations of the backscattering efficiency as a function of particle radius for lignite particles. Simulations consider a log-normal size distribution, with a percentage standard deviation of 5 %. Upper panel: selection of a minimum radius of 1.84 μm, as given by Civiš and Hovorka (2010), and a maximum radius of 10 μm; lower panel: selection of a minimum radius of 8 μm, as given by Triantafyllou *et al.* (2006)), and a maximum radius of 100 μm. Both simulations consider a sounding wavelength of 1.064 ~~mm~~μm.

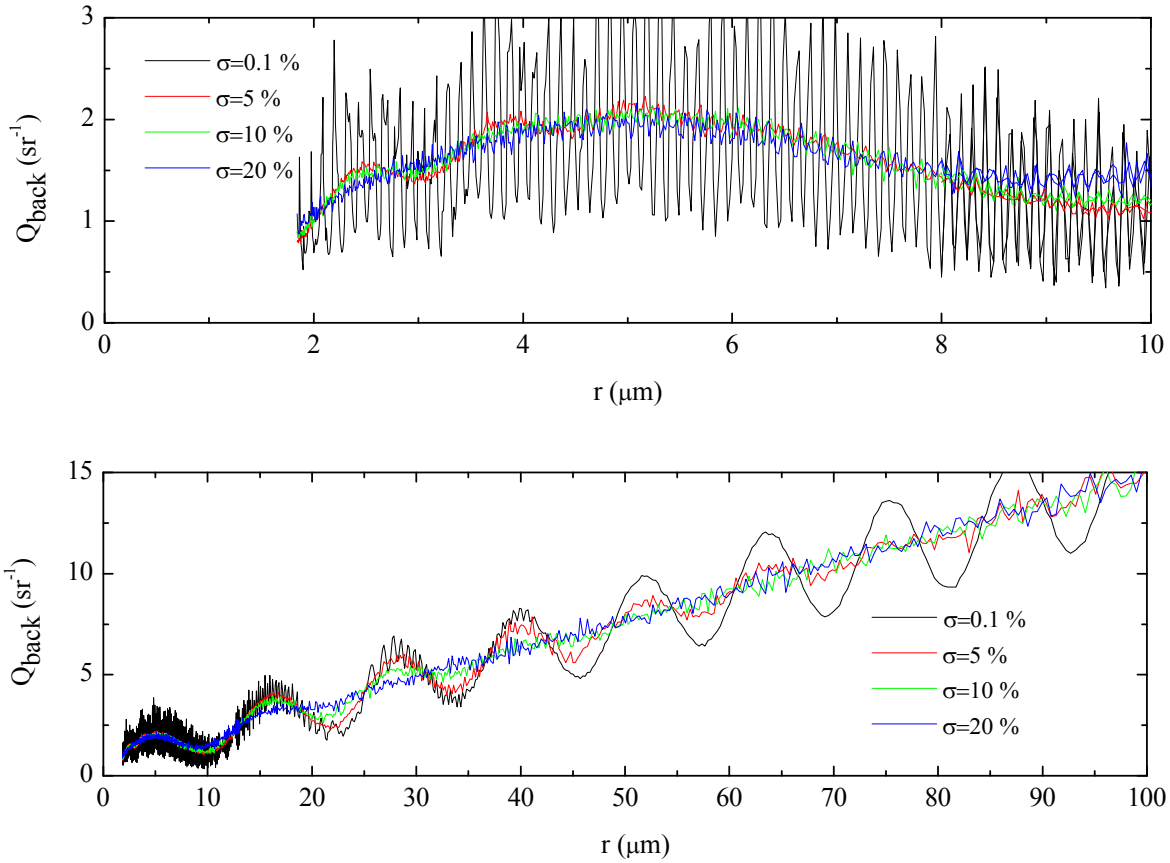

Figure 8: Simulations of the backscattering efficiency at 1064 nm as a function of particle radius for lignite particles, considering a log-normal size distribution with values of σ equal to 0.1, 5, 10 and 20 %. Upper panel: selection of a minimum radius of 1.84 µm, as given by Civiš and Hovorka (2010), and a maximum radius of 10 µm; lower panel: selection of a minimum radius of 8 µm, as given by Triantafyllou *et al.* (2006)), and a maximum radius of 100 µm. Both simulations consider a sounding wavelength of 1.064 µm~~mm~~.